International Journal of Solids and Structures 58 (2015) 270–287

Contents lists available at ScienceDirect

International Journal of Solids and Structures

journal homepage: www.elsevier.com/locate/ijsolstr

Buckling and postbuckling of variable angle tow composite plates under in-plane shear loading

Gangadharan Raju [a], Zhangming Wu [a], Paul M. Weaver [b,*]

[a] Advanced Composite Centre for Innovation and Science, Department of Aerospace Engineering, Queen's Building, University Walk, United Kingdom
[b] Lightweight Structures, Advanced Composite Centre for Innovation and Science, Department of Aerospace Engineering, Queen's Building, University Walk, United Kingdom

ARTICLE INFO

Article history:
Received 3 December 2013
Received in revised form 30 April 2014
Available online 17 January 2015

Keywords:
Buckling
Postbuckling
Variable angle tow composite plates
Differential quadrature method

ABSTRACT

A geometrically nonlinear analysis of symmetric variable angle tow (VAT) composite plates under in-plane shear is investigated. The nonlinear von Karman governing differential equations are derived for postbuckling analysis of symmetric VAT plate structures which are subsequently solved using the differential quadrature method. The effect of in-plane extension-shear coupling on the buckling and postbuckling performance of VAT composite plates is investigated. The buckling and postbuckling behaviour of VAT plates under positive and negative shear is studied for different VAT fibre orientations, aspect ratios, combined axial compression and their performance is compared with that of straight fibre composites. It is shown that there can be enhanced shear buckling and postbuckling performance for both displacement-control and load-control and that the underpinning driving mechanics are different for each.

1. Introduction

Stability analysis of variable angle tow (VAT) composites under compression load has been studied extensively and response has been shown to have superior structural performance over conventional straight fibre composites (Hyer and Lee, 1991; Gurdal and Olmedo, 1993; Gurdal et al., 2008). In this work, the buckling and postbuckling behaviour of VAT plates under in-plane shear is investigated. The concept of tow steering provides more freedom to design light-weight composite structures with improved structural performance when compared to traditional straight fibre designs. Little work has been reported on the stability analysis of VAT plates under shear load. Biggers and Fageau (1994) studied the concept of stiffness tailoring for improving the shear buckling performance of composite plates by redistributing the layups with certain fibre orientations across the planform of the plate. Their study showed a 50% improvement of shear buckling load over straight fibre composites by redistributing ±45 plies along the diagonal directions. Waldhart (1996) used the Rayleigh–Ritz method to study the buckling performance of tow steered VAT plates under uniform end-shortening and in-plane shear load. The effects of extensional-shear coupling (A_{16}, A_{26}) were not considered in their shear buckling study. Nemeth (1997) performed a parametric study on the buckling behaviour of long symmetrical composite plates under shear and reported the effects of membrane anisotropy are more important for shear loaded plates than compression or in-plane bending. Weaver (2004) studied the elastic tailoring of long composite laminates using both flexural and membrane anisotropy and quantified their effects on positive/negative shear buckling behaviour. Wu et al. (2012) studied the buckling performance of VAT plates under compression, shear and combined loading using energy methods. Their study investigated the effect of extensional-shear coupling (A_{16}, A_{26}) and bend-twist coupling (D_{16}, D_{26}) on the buckling behaviour of VAT plates. Lopes et al. (2010) and Gomes et al. (2013) studied the buckling and postbuckling failure response of variable stiffness composites with cut-outs under compression and shear loading, respectively. They used finite element analysis to model the failure of VAT plates which requires significant computational effort. Rahman et al. (2011) studied the postbuckling response of VAT plates using a perturbation approach, coupled with finite element modelling, to generate a reduced-order model for computation of postbuckling coefficients to predict the postbuckling stiffness of VAT plates. Wu et al. (2013) studied the postbuckling performance of VAT plates under axial compression with linear fibre angle variation for different in-plane boundary conditions and proposed different measures to quantify the postbuckling performance of VAT plates.

Numerous studies on VAT plates rely on finite element (FE) modelling for analysis and design of these structures. As a consequence of variable stiffness coefficients, prebuckling stress distributions can be highly nonlinear (spatially) in-plane, even for

* Corresponding author.
E-mail address: paul.weaver@bristol.ac.uk (P.M. Weaver).

http://dx.doi.org/10.1016/j.ijsolstr.2015.01.011
0020-7683/

uniform loading, and not immediately intuitive (Gurdal and Olmedo, 1993V). Furthermore, it is not obvious whether an FE mesh which is converged for prebuckling analysis will also be converged for buckling or for subsequent postbuckling analyses. A further limitation of FE analysis is that rather than modelling continuous fibre paths, the fibre angle distribution is treated as piecewise constant within each element, leading to spurious stress and strain residuals (i.e. noise) in coarse meshes. Therefore, a strong need for developing semi-analytical models that complements finite element analysis for modelling of VAT panel is required. In the present work, numerical methodology based on the differential quadrature method (DQM) is developed for buckling and postbuckling analysis of VAT panels under in-plane shear load. In prior works, the authors have successfully applied DQM for evaluation of buckling and postbuckling behaviour of VAT plates under compression for different plate boundary conditions (Raju et al., 2012, 2013). DQM, as a numerical tool, has been shown to be accurate and require less degrees of freedom than FE for solving the buckling and postbuckling problem of VAT panels. Once simple geometries in FE analysis have been validated by DQM models, then the designer can proceed with increased confidence to more complicated geometries and loads. More importantly still, is the physical insight gained in stress redistribution tailoring, and the ability to massage buckling phenomena to be more benign.

In the present work, the underlying mechanics behind the improvement of shear buckling and postbuckling behaviour of VAT plates with linear fibre angle variation is studied. The effect of in-plane extension-shear coupling on the buckling and postbuckling performance of VAT composite plates is investigated for different in-plane boundary conditions. Furthermore, the effect of direction of the applied shear on the postbuckling behaviour of VAT plates under compression is also discussed.

2. Differential quadrature method

In the differential quadrature method, the derivative of a function, with respect to a space variable at a given discrete grid point, is approximated as a weighted linear sum of the function values at all of the grid points in the entire domain of that variable (Bellman and Casti, 1971). The nth order partial derivative of a function $f(x)$ at the ith discrete point is approximated by

$$\frac{\partial^n f(x_i)}{\partial x^n} = A_{ij}^{(n)} f(x_j) \quad i = 1, 2, \ldots, N_x, \tag{1}$$

where x_i = set of discrete points in the x direction; and $A_{ij}^{(n)}$ are the weighting coefficients of the nth derivative and repeated index j indicates summation from 1 to N_x. The partial derivatives of a function $f(x,y)$ in matrix form are given by,

$$\begin{aligned}
&\frac{\partial f}{\partial x} = P_x f, \quad \frac{\partial f}{\partial y} = f P_y^T, \quad \frac{\partial f}{\partial x \partial y} = P_x f P_y^T,\\
&\frac{\partial^2 f}{\partial x^2} = Q_x f, \quad \frac{\partial^2 f}{\partial y^2} = f Q_y^T, \quad \frac{\partial^4 f}{\partial x^2 \partial y^2} = Q_x f Q_y^T,\\
&\frac{\partial^3 f}{\partial x^3} = R_x f, \quad \frac{\partial^3 f}{\partial y^3} = f R_y^T, \quad \frac{\partial^4 f}{\partial x^4} = S_x f, \quad \frac{\partial^4 f}{\partial y^4} = f S_y^T,
\end{aligned} \tag{2}$$

where P, Q, R, S with subscripts x, y are the DQM weighting coefficient matrices for the first, second, third, and fourth order partial derivatives with respect to x and y directions, respectively. The unknown function f is expressed in matrix form along the two-dimensional grid, as shown in Fig. 1 and superscript T represents the transpose of the matrix. The domain grid points refer to the points where the governing partial differential equations are expressed in DQM form and the boundary grid points refer to the points where multiple boundary conditions are applied (Fig. 1). The information regarding the grid distribution for computation of weighting coefficient matrices and modelling multiple boundary conditions are explained, in detail, in the textbook by Shu (2000).

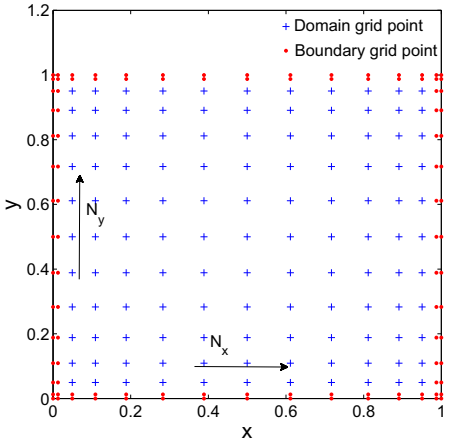

Fig. 1. DQM grid distribution in two-dimension.

3. Postbuckling analysis of VAT panels

In symmetric VAT panels, stiffness (A, D matrices) varies with x–y coordinates and the constitutive equation in partial inverse form is given by,

$$\begin{Bmatrix} \epsilon^0 \\ M \end{Bmatrix} = \begin{bmatrix} A^*(x,y) & 0 \\ 0 & D(x,y) \end{bmatrix} \begin{Bmatrix} \overline{N} \\ \kappa \end{Bmatrix}, \tag{3}$$

where $\overline{N}$, M are the stress and moment resultants, $A^* = A^{-1}$ is the compliance matrix and D is the bending stiffness matrix. The nonlinear midplane strains ϵ^0 and curvatures κ are defined as

$$\begin{aligned}
&\epsilon_x^0 = u_{,x} + \frac{1}{2} w_{,x}^2 + w_{,x} w_{0,x}, \quad \epsilon_y^0 = v_{,y} + \frac{1}{2} w_{,y}^2 + w_{,y} w_{0,y},\\
&\epsilon_{xy}^0 = u_{,y} + v_{,x} + w_{,x} w_{,y} + w_{,x} w_{0,y} + w_{,y} w_{0,x},\\
&\kappa_x = -w_{,xx}, \quad \kappa_y = -w_{,yy}, \quad \kappa_{xy} = -2 w_{,xy}
\end{aligned} \tag{4}$$

where u, v, w are the displacements and w_0 is the initial imperfection function. A stress function Ω is introduced such that the stress resultants are defined by,

$$\overline{N}_x = \Omega_{,yy}, \quad \overline{N}_y = \Omega_{,xx}, \quad \overline{N}_{xy} = -\Omega_{,xy}. \tag{5}$$

The compatibility condition in terms of mid-plane strains in a plane stress condition is given by (Whitney, 1987)

$$\begin{aligned}
\epsilon_{x,yy}^0 + \epsilon_{y,xx}^0 - \epsilon_{xy,xy}^0 = {} & w_{,xy}^2 - w_{,xx} w_{,yy} + 2 w_{,xy} w_{0,xy} - w_{,xx} w_{0,xx}\\
& - w_{,yy} w_{0,xx}.
\end{aligned} \tag{6}$$

After substitution of Eqs. (3)–(5) into Eq. (6), the final form is given by

$$\begin{aligned}
&A_{11}^*(x,y)\Omega_{,yyyy} - 2A_{16}^*(x,y)\Omega_{,xyyy} + (2A_{12}^*(x,y) + A_{66}^*(x,y))\Omega_{,xxyy}\\
&\quad - 2A_{26}^*(x,y)\Omega_{,xxxy} + A_{22}^*(x,y)\Omega_{,xxxx} + (2A_{11,y}^*(x,y)\\
&\quad - A_{16,x}^*(x,y))\Omega_{,yyy} + (2A_{12,x}^*(x,y) - 3A_{16,y}^*(x,y)\\
&\quad + A_{66,x}^*(x,y))\Omega_{,xyy} + (2A_{12,y}^*(x,y) - 3A_{26,x}^*(x,y)\\
&\quad + A_{66,y}^*(x,y))\Omega_{,xxy} + (2A_{22,x}^*(x,y) - A_{26,y}^*(x,y))\Omega_{,xxx}\\
&\quad + (A_{11,yy}^*(x,y) + A_{12,xx}^*(x,y) - A_{16,xy}^*(x,y))\Omega_{,yy} + (-A_{26,xx}^*(x,y)\\
&\quad - A_{16,yy}^*(x,y) + A_{66,xy}^*(x,y))\Omega_{,xy} + (A_{12,yy}^*(x,y) + A_{22,xx}^*(x,y)\\
&\quad - A_{26,xy}^*(x,y))\Omega_{,xx}\\
&\quad = w_{,xy}^2 - w_{,xx} w_{,yy} + 2 w_{,xy} w_{0,xy} - w_{,xx} w_{0,xx} - w_{,yy} w_{0,xx}.
\end{aligned} \tag{7}$$

The differential equation of transverse motion that governs the postbuckling analysis of a symmetrical VAT plate is given by,

$$\frac{\partial^2 M_x}{\partial x^2}+2\frac{\partial^2 M_{xy}}{\partial x\partial y}+\frac{\partial^2 M_y}{\partial y^2}+\overline{N}_x\left(\frac{\partial^2 w}{\partial x^2}+\frac{\partial^2 w_0}{\partial x^2}\right)+2\overline{N}_{xy}\left(\frac{\partial^2 w}{\partial x\partial y}+\frac{\partial^2 w_0}{\partial x\partial y}\right)+\overline{N}_y\left(\frac{\partial^2 w}{\partial y^2}+\frac{\partial^2 w_0}{\partial y^2}\right)+q=0, \tag{8}$$

where M_x, M_y, M_{xy} are the moment distributions and q is the load applied in z direction (Whitney, 1987). Eqs. (3)–(5) are then substituted into Eq. (8) and the resulting differential equation is given by

$$\begin{aligned}&D_{11}(x,y)w_{,xxxx}+4D_{16}(x,y)w_{,xxxy}+2(D_{12}(x,y)+2D_{66}(x,y))w_{,xxyy}\\&+4D_{26}(x,y)w_{,yyyx}+D_{22}(x,y)w_{,yyyy}+2(D_{11,x}(x,y)\\&+D_{16,y}(x,y))w_{,xxx}+(6D_{16,x}(x,y)+2D_{12,y}(x,y)+4D_{66,y}(x,y))w_{,xxy}\\&+(2D_{12,x}(x,y)+4D_{66,x}(x,y)+6D_{26,y}(x,y))w_{,xyy}+2(D_{26,x}(x,y)\\&+D_{22,y}(x,y))w_{,yyy}+(D_{11,xx}(x,y)+2D_{16,xy}(x,y)+D_{12,yy}(x,y))w_{,xx}\\&+(2D_{16,xx}(x,y)+4D_{66,xy}(x,y)+2D_{26,yy}(x,y))w_{,xy}+(D_{12,xx}(x,y)\\&+2D_{26,xy}(x,y)+D_{22,yy}(x,y))w_{,yy}-\Omega_{yy}(w_{,xx}+w_{0,xx})\\&+2\Omega_{xy}(w_{,xy}+w_{0,xy})-\Omega_{xx}(w_{,yy}+w_{0,yy})+q=0.\end{aligned} \tag{9}$$

Thus, Eqs. (7) and (9) represent coupled fourth order nonlinear elliptic partial differential equation in terms of stress function Ω and transverse deflection w with variable coefficients for postbuckling analysis of VAT composite plates. The stress function boundary conditions are given by

$$\begin{aligned}&\Omega_{,yy}|_{x=0,a}=0,\quad \Omega_{,xx}|_{y=0,b}=0,\quad \Omega_{,xy}|_{x=0,a;y=0,b}=P_{xy},\\&\Omega|_{x=0,y=0}=\Omega_{,x}|_{x=0,y=0}=\Omega_{,y}|_{x=0,y=0}=0.\end{aligned} \tag{10}$$

where P_{xy} is the applied shear load. The boundary conditions expressed in terms of Ω represent uniform shear applied all along the edges of the plate. The simply supported plate boundary conditions are given by,

$$\begin{aligned}&x=0,a;\quad w=0;\\&M_x=-D_{11}(x,y)w_{,xx}-D_{12}(x,y)w_{,yy}-2D_{16}(x,y)w_{,xy}=0\\&y=0,b;\quad w=0;\\&M_y=-D_{12}(x,y)w_{,xx}-D_{22}(x,y)w_{,yy}-2D_{26}(x,y)w_{,xy}=0.\end{aligned} \tag{11}$$

Chen et al. (2000) used DQM to solve the geometrically nonlinear bending problem of isotropic and orthotropic rectangular plates. Taheri and Moradi (2000) applied DQM to perform postbuckling analysis of straight fibre composites and used an arclength approach to solve the nonlinear algebraic equations. In their works, the nonlinear GDEs were written in terms of displacements (u, v, w) and DQM was subsequently applied to solve them. Whilst studying the nonlinear bending of orthotropic plates, the Hadamard product ($\circ$), Kronecker product ($\otimes$) and SJT product ($\diamondsuit$) of matrices were used by Chen et al. (Chen et al., 2000) to simplify the DQM form of governing differential equations. Consider matrices A, B of size $m\times n$, the Hadamard product $A\circ B$ is a matrix of the same dimensions with elements given by

$$(A\circ B)_{ij}=A_{ij}\cdot B_{ij} \tag{12}$$

Similarly, given a $m\times n$ matrix A and a $p\times q$ matrix B, the Kronecker product $A\otimes B$ is a matrix of size $mp\times nq$ given by

$$A\otimes B=\begin{bmatrix}a_{11}B & \cdots & a_{1n}B\\ \vdots & \ddots & \vdots\\ a_{m1}B & \cdots & a_{mn}B\end{bmatrix} \tag{13}$$

The SJT product ($\diamondsuit$) between a matrix A of size $m\times n$ and a vector $\vec{v}$ of size $m\times 1$ results in a matrix of same size as A and is expressed as

$$A\diamondsuit\vec{v}=A\cdot(I\cdot\vec{v}) \tag{14}$$

where I is the identity matrix. Chu (2009) applied a similar direct matrix product, equivalent to Chen's approach, to solve nonlinear integro-differential equations. In the present work, the Kronecker, Hadamard and SJT matrix products are applied to the coupled nonlinear postbuckling equations (Eqs. (7) and (9)) and the DQM form of these expressions are given by,

$$\begin{aligned}&\left(\vec{A}^*_{11}\otimes\vec{J}\right)\circ(I_y\otimes S_y)\vec{\Omega}-\left(2\vec{A}^*_{16}\otimes\vec{J}\right)\circ(P_x\otimes R_y)\vec{\Omega}\\&+\left(\left(2\vec{A}^*_{12}+\vec{A}^*_{66}\right)\otimes\vec{J}\right)\circ(Q_x\otimes Q_y)\vec{\Omega}-\left(2\vec{A}^*_{26}\otimes\vec{J}\right)\circ(R_x\otimes P_y)\vec{\Omega}\\&+(\vec{A}^*_{22}\otimes\vec{J})\circ(S_x\otimes I_x)\vec{\Omega}+\left(\left(2\vec{A}^*_{11,y}-\vec{A}^*_{16,x}\right)\otimes\vec{J}\right)\circ(I_y\otimes R_y)\vec{\Omega}\\&+\left(\left(2\vec{A}^*_{12,x}-3\vec{A}^*_{16,y}+\vec{A}^*_{66,x}\right)\otimes\vec{J}\right)\circ(P_x\otimes Q_y)\vec{\Omega}\\&+\left(\left(2\vec{A}^*_{12,y}-3\vec{A}^*_{26,x}+\vec{A}^*_{66,y}\right)\otimes\vec{J}\right)\circ(Q_x\otimes P_y)\vec{\Omega}\\&+\left(\left(2\vec{A}^*_{22,x}-\vec{A}^*_{26,y}\right)\otimes\vec{J}\right)\circ(R_x\otimes I_x)\vec{\Omega}\\&+\left(\left(\vec{A}^*_{11,yy}+\vec{A}^*_{12,xx}-\vec{A}^*_{16,xy}\right)\otimes\vec{J}\right)\circ(I_y\otimes Q_y)\vec{\Omega}\\&+\left(\left(-\vec{A}^*_{26,xx}-\vec{A}^*_{16,yy}+\vec{A}^*_{66,xy}\right)\otimes\vec{J}\right)\circ(P_x\otimes P_y)\vec{\Omega}\\&+\left(\left(\vec{A}^*_{12,yy}+\vec{A}^*_{22,xx}-\vec{A}^*_{26,xy}\right)\otimes\vec{J}\right)\circ(Q_x\otimes I_x)\vec{\Omega}\\&=((P_x\otimes P_y)\vec{w})\circ((P_x\otimes P_y)\vec{w})-((Q_x\otimes I_x)\vec{w})\circ((I_y\otimes Q_y)\vec{w})\\&+2((P_x\otimes P_y)\vec{w})\circ((P_x\otimes P_y)\vec{w}_0)-((Q_x\otimes I_x)\vec{w})\circ((I_y\otimes Q_y)\vec{w}_0)\\&-((I_y\otimes Q_y)\vec{w})\circ((Q_x\otimes I_x)\vec{w}_0),\end{aligned} \tag{15}$$

$$\begin{aligned}&(\vec{D}_{11}\otimes\vec{J})\circ(S_x\otimes I_x)\vec{w}+(4\vec{D}_{16}\otimes\vec{J})\circ(R_x\otimes P_y)\vec{w}\\&+(2(\vec{D}_{12}+2\vec{D}_{66})\otimes J)\circ(Q_x\otimes Q_y)\vec{w}+(4\vec{D}_{26}\otimes\vec{J})\circ(R_x\otimes P_y)\vec{w}\\&+(\vec{D}_{22}\otimes\vec{J})\circ(I_y\otimes S_y)\vec{w}+(2(\vec{D}_{11,x}+\vec{D}_{16,y})\otimes\vec{J})\circ(R_x\otimes I_x)\vec{w}\\&+((6\vec{D}_{16,x}+2\vec{D}_{12,y}+4\vec{D}_{66,y})\otimes\vec{J})\circ(Q_x\otimes P_y)\vec{w}\\&+((2\vec{D}_{12,x}+4\vec{D}_{66,x}+6\vec{D}_{26,y})\otimes\vec{J})\circ(P_x\otimes Q_y)\vec{w}\\&+(2(\vec{D}_{26,x}+\vec{D}_{22,y})\otimes\vec{J})\circ(I_y\otimes R_y)\vec{w}\\&+((\vec{D}_{11,xx}+2\vec{D}_{16,xy}+\vec{D}_{12,yy})\otimes\vec{J})\circ(Q_x\otimes I_x)\vec{w}\\&+((2\vec{D}_{16,xx}+4\vec{D}_{66,xy}+2\vec{D}_{26,yy})\otimes\vec{J})\circ(P_x\otimes Q_y)\vec{w}\\&+((\vec{D}_{12,xx}+2\vec{D}_{26,xy}+\vec{D}_{22,yy})\otimes\vec{J})\circ(I_y\otimes Q_y)\vec{w}\\&-(I_y\otimes B_y)\vec{\Omega}(Q_x\otimes I_x)(\vec{w}+\vec{w}_0)+2(P_x\otimes P_y)\vec{\Omega}(P_x\otimes P_y)(\vec{w}+\vec{w}_0)\\&-(Q_x\otimes I_x)\vec{\Omega}(I_y\otimes Q_y)(\vec{w}+\vec{w}_0)+\vec{q}=0,\end{aligned} \tag{16}$$

where $\vec{\Omega}$, $\vec{w}$, $\vec{w}_0$, $\vec{q}$, $\vec{A}^*_{ij}$, $\vec{D}_{ij}$ $(i,j=1,2,6)$ are vectors generated by stacking the columns of the corresponding matrices Ω, w, w_0, q, A^*_{ij}, D_{ij}, $\vec{J}=[1,1,\ldots,1]_{1\times N}$ is a row vector, $N=N_x+N_y$ represents the total number of grid points in the two-dimensional domain and N_x, N_y represent the number of grid points along the x and y directions. The size of the identity matrices I_x, I_y depends on N_x and N_y, respectively. Eqs. (15) and (16) are further simplified into matrix forms given by

$$\begin{aligned}&L_1\vec{\Omega}=(L_2\vec{w})\circ(L_2\vec{w})-(L_3\vec{w})\circ(L_4\vec{w})+2(L_2\vec{w})\circ(L_2\vec{w}_0)\\&\qquad-(L_3\vec{w})\circ(L_4\vec{w}_0)-(L_4\vec{w})\circ(L_3\vec{w}_0),\\&L_5\vec{w}-(L_6\vec{\Omega})\circ(L_3(\vec{w}+\vec{w}_0))+2(L_7\vec{\Omega})\circ(L_2(\vec{w}+\vec{w}_0))\\&\qquad-(L_8\vec{\Omega})\circ(L_4(\vec{w}+\vec{w}_0))+\vec{q}=0.\end{aligned} \tag{17}$$

The matrix operators in Eq. (17) are given by,

$$
\begin{aligned}
L_1 &= (\vec{A}^*_{11}\otimes\vec{J})\circ(I_y\otimes S_y) - (2\vec{A}^*_{16}\otimes\vec{J})\circ(P_x\otimes R_y)\\
&\quad + ((2\vec{A}^*_{12}+\vec{A}^*_{66})\otimes\vec{J})\circ(Q_x\otimes Q_y) - (2\vec{A}^*_{26}\otimes\vec{J})\circ(R_x\otimes P_y)\\
&\quad + (\vec{A}^*_{22}\otimes\vec{J})\circ(S_x\otimes I_x) + ((2\vec{A}^*_{11,y}-\vec{A}^*_{16,x})\otimes\vec{J})\circ(I_y\otimes R_y)\\
&\quad + ((2\vec{A}^*_{12,x}-3\vec{A}^*_{16,y}+\vec{A}^*_{66,x})\otimes\vec{J})\circ(P_x\otimes Q_y)\\
&\quad + ((2\vec{A}^*_{12,y}-3\vec{A}^*_{26,x}+\vec{A}^*_{66,y})\otimes\vec{J})\circ(Q_x\otimes P_y)\\
&\quad + ((2\vec{A}^*_{22,x}-\vec{A}^*_{26,y})\otimes\vec{J})\circ(R_x\otimes I_x)\\
&\quad + ((\vec{A}^*_{11,yy}+\vec{A}^*_{12,xx}-\vec{A}^*_{16,xy})\otimes\vec{J})\circ(I_y\otimes Q_y)\\
&\quad + ((-\vec{A}^*_{26,xx}-\vec{A}^*_{16,yy}+\vec{A}^*_{66,xy})\otimes\vec{J})\circ(P_x\otimes P_y)\\
&\quad + ((\vec{A}^*_{12,yy}+\vec{A}^*_{22,xx}-\vec{A}^*_{26,xy})\otimes\vec{J})\circ(Q_x\otimes I_x),\\
L_2 &= P_x\otimes P_y,\quad L_3 = Q_x\otimes I_x,\quad L_4 = I_y\otimes Q_y,\\
L_5 &= (\vec{D}_{11}\otimes\vec{J})\circ(S_x\otimes I_x) + (4\vec{D}_{16}\otimes\vec{J})\circ(R_x\otimes P_y)\\
&\quad + (2(\vec{D}_{12}+2\vec{D}_{66})\otimes J)\quad\circ(Q_x\otimes Q_y) + (4\vec{D}_{26}\otimes\vec{J})\circ(R_x\otimes P_y)\\
&\quad + (\vec{D}_{22}\otimes\vec{J})\circ(I_y\otimes S_y)\quad + (2(\vec{D}_{11,x}+\vec{D}_{16,y})\otimes\vec{J})\circ(R_x\otimes I_x)\\
&\quad + ((6\vec{D}_{16,x}+2\vec{D}_{12,y}+4\vec{D}_{66,y})\otimes\vec{J})\circ(Q_x\otimes P_y)\\
&\quad + ((2\vec{D}_{12,x}+4\vec{D}_{66,x}+6\vec{D}_{26,y})\otimes\vec{J})\circ(P_x\otimes Q_y)\\
&\quad + (2(\vec{D}_{26,x}+\vec{D}_{22,y})\otimes\vec{J})\circ(I_y\otimes R_y)\\
&\quad + ((\vec{D}_{11,xx}+2\vec{D}_{16,xy}+\vec{D}_{12,yy})\otimes\vec{J})\circ(Q_x\otimes I_x)\\
&\quad + ((2\vec{D}_{16,xx}+4\vec{D}_{66,xy}+2\vec{D}_{26,yy})\otimes\vec{J})\circ(P_x\otimes P_y)\\
&\quad + ((\vec{D}_{12,xx}+2\vec{D}_{26,xy}+\vec{D}_{22,yy})\otimes\vec{J})\circ(I_y\otimes Q_y),\\
L_6 &= I_y\otimes Q_y,\quad L_7 = P_x\otimes P_y,\quad L_8 = Q_x\otimes I_x,
\end{aligned}
\tag{18}
$$

where $\otimes$ is the Kronecker matrix product and $\circ$ is the Hadamard matrix product and all the matrix operators are of size $N\times N$. Various methods have been reported previously for implementation of multiple boundary conditions along the plate edges using DQM (Shu, 2000). In the current work, the direct substitution method proposed by Shu and Du (1997, 1999) has been used to implement the different combination of plate boundary conditions. Using this approach, the boundary conditions for stress function and transverse displacement were applied to the boundary grid points in the DQM domain. The values at the boundary grid points were expressed in terms of unknown domain grid point values. The modified matrices are reduced to size $N_d\times N_d$ where N_d represent the total number of domain points and the modified DQM equations are given by,

$$
\begin{aligned}
\vec{\Omega}_d(\vec{w}_d) &= \bar{L}_1^{-1}((\bar{L}_2\vec{w}_d)\circ(\bar{L}_2\vec{w}_d) - (\bar{L}_3\vec{w}_d)\circ(\bar{L}_4\vec{w}_d) + 2(\bar{L}_2\vec{w}_d)\circ(\bar{L}_2\vec{w}_{0d})\\
&\quad - (\bar{L}_3\vec{w}_d)\circ(\bar{L}_4\vec{w}_{0d}) - (\bar{L}_4\vec{w}_d)\circ(\bar{L}_3\vec{w}_{0d})),\\
\Phi(\vec{w}_d) &= \bar{L}_5\vec{w}_d - (\bar{L}_6\vec{\Omega}_d)\circ(\bar{L}_3(\vec{w}_d+\vec{w}_{0d})) + 2(\bar{L}_7\vec{\Omega}_d)\circ(\bar{L}_2(\vec{w}_d+\vec{w}_{0d}))\\
&\quad - (\bar{L}_8\vec{\Omega}_d)\circ(\bar{L}_4(\vec{w}_d+\vec{w}_{0d})) + \vec{q}_d = 0,
\end{aligned}
\tag{19}
$$

which represent the nonlinear algebraic DQM equations as a function of transverse displacement ($\vec{w}_d$) and were solved using a Newton–Raphson algorithm. The Jacobian of these equations with respect to $\vec{w}_d$ is obtained using the SJT matrix product as,

$$
\begin{aligned}
\frac{\partial\vec{\Omega}_d(\vec{w}_d)}{\partial\vec{w}_d} &= \bar{L}_1^{-1}(2\bar{L}_2\diamondsuit(\bar{L}_2\vec{w}_d) - (\bar{L}_3\diamondsuit\bar{L}_3\vec{w}_d + \bar{L}_4\diamondsuit\bar{L}_3\vec{w}_d)\\
&\quad + 2(\bar{L}_2\diamondsuit\bar{L}_2\vec{w}_{0d}) - (\bar{L}_3\diamondsuit\bar{L}_4\vec{w}_{0d})\\
&\quad - (\bar{L}_4\diamondsuit\bar{L}_3\vec{w}_{0d})),\quad \frac{\partial\Phi(\vec{w}_d)}{\partial\vec{w}_d}\\
&= \bar{L}_5 - \left(\bar{L}_6\frac{\partial\vec{\Omega}_d}{\partial\vec{w}_d}\diamondsuit\bar{L}_3(\vec{w}_d+\vec{w}_{0d}) + \bar{L}_3\diamondsuit\bar{L}_6\vec{\Omega}_d\right)\\
&\quad + 2\left(\bar{L}_7\frac{\partial\vec{\Omega}_d}{\partial\vec{w}_d}\diamondsuit\bar{L}_2(\vec{w}_d+\vec{w}_{0d}) + \bar{L}_2\diamondsuit\bar{L}_7\vec{\Omega}_d\right)\\
&\quad - \left(\bar{L}_8\frac{\partial\vec{\Omega}_d}{\partial\vec{w}_d}\diamondsuit\bar{L}_4(\vec{w}_d+\vec{w}_{0d}) + \bar{L}_4\diamondsuit\bar{L}_8\vec{\Omega}_d\right).
\end{aligned}
\tag{20}
$$

The SJT product allows computation of the Jacobian for discretized nonlinear partial differential equations similar to calculation of derivative of a single variable scalar function. The SJT approach facilitates fast and accurate evaluation of the Jacobian matrix and the Newton–Raphson iteration approach is used to determine the nonlinear displacement field

$$
\vec{w}_d^{(i+1)} = \vec{w}_d^{(i)} - \left(\frac{\partial\Phi(\vec{w}_d^{(i)})}{\partial\vec{w}_d}\right)^{-1}\Phi(\vec{w}_d^{(i)}),
\tag{21}
$$

The Newton–Raphson algorithm ensures quadratic convergence and requires few iterations to converge for each load step applied in the nonlinear postbuckling regime.

4. Problem definition

The VAT plates considered are symmetrically laminated and the material properties for each lamina are given by $E_1 = 181$ GPa, $E_2 = 10.27$ GPa, $G_{12} = 7.17$ GPa, $\nu_{12} = 0.28$ with lamina thickness $t = 1.272$ mm and number of laminae, $n = 8$. The VAT plate with linear angle variation along the x direction is given by

$$
\theta(x) = \phi + \frac{2(T_1 - T_0)}{a}|x| + T_0,
\tag{22}
$$

where ϕ is the angle of rotation, T_0 is the fibre orientation angle at the panel center $x = 0$, and T_1 is the fiber orientation angle at the panel ends $x = \pm a/2$ (see Fig. 2). The non-uniform grid distribution given by the Chebyshev–Gauss–Labotto points are used for the computation of weighting matrices and is given by

$$
X_i = \frac{1}{2}\left[1 - \cos\left(\frac{i-1}{N-1}\pi\right)\right],\quad i = 1,2,\ldots N,
\tag{23}
$$

where N is the number of grid points. In order to validate the DQM results, finite element modelling of the VAT panels was carried out using ABAQUS. The S4 shell element was chosen for discretization of the VAT plate structure. To achieve good accuracy, mesh sizes of 40×40, 90×30 were selected for plates with aspect ratio 1 and 3, respectively. Using the linear fibre angle definition, fibre orientation was evaluated at the centroid of each element. The material properties for elements were then defined using the fibre orientation information. Prior to the buckling analysis, in-plane analysis of the VAT laminates under shear was carried out to compute the stress resultant distributions. The in-plane analysis results

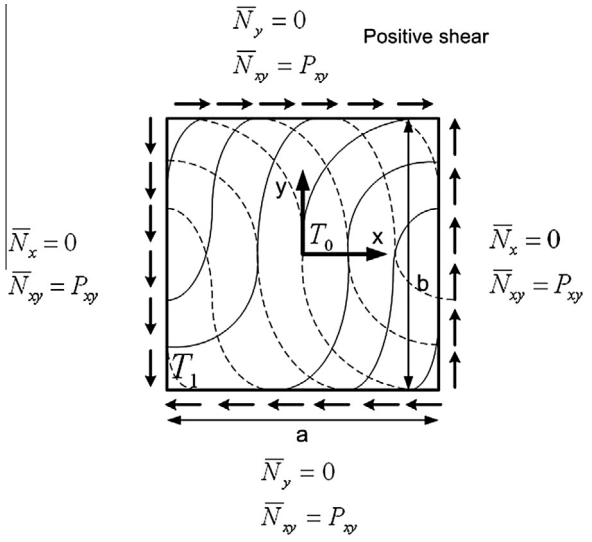

Fig. 2. Square VAT plate subjected to positive in-plane shear load.

were then used in the buckling analysis for evaluating the critical shear buckling load efficient. The postbuckling of VAT plates was then performed using buckling analysis results. The imperfection function required for nonlinear FE analysis was chosen to be the first buckling mode shape. The imperfection magnitude was taken to be one percent of the plate thickness and the arc length parameters required for Riks analysis were adapted to the particular VAT configuration that was studied. All plates considered in this study were considered to be simply supported.

Buckling results are normalised with respect to that of a homogeneous quasi-isotropic (QI) laminate. The laminates $[45/-45/0/90]_s$, $[90/0/45/-45]_s$ are commonly termed QI, yet they contain different amounts of flexural anisotropy (Diaconu and Weaver, 2006). To nullify the effects of flexural anisotropy we have chosen a layup of 48 layers comprising $0,\ 90,\ \pm 45$ fibre orientations. Alternatively, the homogeneous QI laminate with equivalent Young's modulus E_{iso}, Poisson's ratio v_{iso} and bending stiffness D_{iso} are given by (Pandey and Sherbourne, 1993; Weaver and Nemeth, 2007),

$$D_{iso} = \frac{E_{iso}h^3}{12(1-v_{iso}^2)}, \quad v_{iso} = \frac{U_4}{U_1}, \quad E_{iso} = U_1(1-v_{iso}^2), \tag{24}$$

where $U_1,\ U_2,\ U_4$ are material invariants (Jones, 1998). The critical buckling load $\overline{N}_{xycr}$ is normalised with respect to the critical buckling state $\overline{N}^{iso}_{xycr}$ of a homogeneous QI laminate. In the numerical study, the effects of in-plane extension-shear coupling $A_{16},\ A_{26}$ on the shear buckling and postbuckling performance of VAT composite plates are investigated.

5. Results and discussion

5.1. Buckling analysis under in-plane shear load

The buckling problem of VAT plates was solved by neglecting the nonlinear terms in Eq. (9) and DQM was then applied to solve the resulting governing differential equations. Initially, the effect of direction of shear load on the buckling behaviour of unidirectional composite plates with different fibre angle orientations and aspect ratios was studied. The DQM simulation was carried out using $N_x = N_y = 19$ grid points for square plate ($a = b$=0.254 m, thickness = 1 mm) and $N_x = N_y = 21$ grid points for a rectangular plate with aspect ratio = 3 (a = 0.762 m, b = 0.254 m, thickness = 1 mm). The normalised buckling load obtained using DQM is shown in Fig. 3. The buckling loads obtained under negative shear are higher than positive shear and this behaviour can be attributed to the alignment of compressive force in the fibre direction by the applied negative shear load. For square and rectangular plates, the 45° and 60° layup respectively, show higher shear buckling performance compared to all other fibre orientations.

Next, the buckling performance of VAT plates under shear load was studied for different linearly varying fibre angle distributions. The DQM grid size was chosen to be $N_x = N_y = 19$ for a square plate ($a = b$=0.254 m, thickness = 1 mm) and $N_x = N_y = 21$ for a plate with aspect ratio = 3 (a = 0.762 m, b = 0.254 m, thickness = 1 mm) based on convergence studies. The normalised shear buckling load evaluated using DQM is shown in Fig. 4 for VAT plates with $\phi = 0$ and various values of $T_0,\ T_1$. In the case of square plates, the straight fibre layup $[45, -45]_{2s}$ shows higher buckling load for both positive and negative shear when compared to all other VAT layups. For composite plates with aspect ratio = 3, the straight fibre layup $[60, -60]_{2s}$ exhibits high buckling load for both positive and negative shear. Fig. 5 shows the buckling load results for VAT plates with $\phi = 45$ and different values of $T_0,\ T_1$. For square plates under negative shear, the straight fibre layup $[45]_8$ shows higher buckling coefficient of 1.91 compared to all VAT plates. This is mainly because the laminate $[45]_8$ is unbalanced and the finite extensional-shear coupling stiffness coefficients $A_{16},\ A_{26}$ introduce $\overline{N}_x,\ \overline{N}_y$ distributions which enhances the negative shear buckling performance. However, for rectangular plates, the VAT layups $(45 \pm \langle 45|0\rangle_{2s}, 45 \pm \langle 50|0\rangle_{2s})$ shows high buckling load compared to all other layups. The improvement in buckling performance of VAT plates under constant shear load is not as significant as observed under axial compression (Raju et al., 2012).

Furthermore, we studied the effect of $A_{16},\ A_{26}$ coefficients on the shear buckling performance by choosing symmetric unbalanced laminates containing both straight fibre and VAT layups. For the numerical study, the square plate with layup configuration $[45_2, 45 \pm \langle T_0|T_1\rangle]_s$ was considered and the normalised buckling load results are shown in Fig. 6. The buckling results for negative shear clearly shows that many layups attain higher values than straight fibre designs, whereas the results under positive shear are not as high compared to negative shear. The reason is due to the compressive component of the applied negative shear load acting along the 45° straight fibre direction. In addition, the added 45 layers to the VAT layups make the laminate unbalanced and introduces non-zero extensional-shear coupling stiffness coefficient $A_{16},\ A_{26}$ distributions. These $A_{16},\ A_{26}$ distributions result in secondary stress resultant states in the plate which aids the buckling resistance in the negative shear direction. If the straight fibre and VAT layups are rotated by 90°, the buckling performance under positive shear will be higher than straight fibre layups, but result

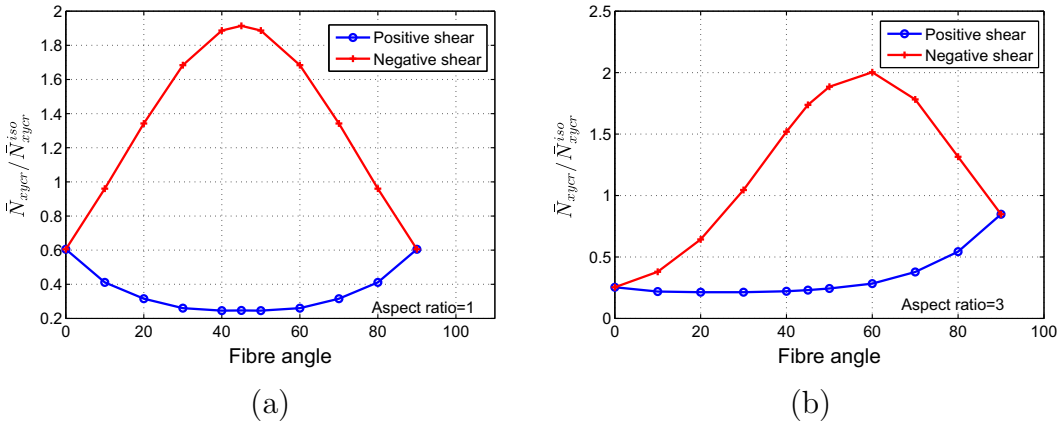

Fig. 3. Unidirectional composite plate subjected to in-plane shear load: (a) Square plate (b) Rectangular plate (Aspect ratio = 3).

in the reduction of buckling performance under negative shear. The composite layup $[45_2, 45 \pm \langle 90|0\rangle]_s$ exhibits a high normalised buckling coefficient equal to 3.23 compared to all other layups, under negative shear. The in-plane stress resultant distributions and buckling mode shape computed using DQM and FE modelling for the $[45_2, 45 \pm \langle 90|0\rangle]_s$ layup are shown in Fig. 7. The DQM results correlate well with FE and requires fewer grid points (19×19) than FE mesh density (40×40). The stress resultant distributions $\overline{N}_x$, $\overline{N}_y$ for the layup $[45_2, 45 \pm \langle 90|0\rangle]_s$ show nonuniform tensile stress in the middle of the plate due to the chosen fibre path and these secondary tensile forces offer additional resistance to buckling under negative shear. The $\overline{N}_{xy}$ distribution for the layup $[45_2, 45 \pm \langle 90|0\rangle]_s$ shows little redistribution of the shear load from the centre of the plate to the edges. However, if the unbalanced layup effects due to addition of 45° layups is eliminated by making the A_{16}, A_{26} distributions equal to zero, the computed normalised shear buckling coefficient is 2.61 and reduction of 19.2% in the buckling coefficient is observed. Thus, the 45° straight fibre layups in the $[45_2, 45 \pm \langle 90|0\rangle]_s$ laminate resists the primary compressive load and when combined with the VAT layups are responsible for the induced secondary tensile stress state in the laminate. Both straight and VAT fibre layups complement each other for the improvement of shear buckling performance. Thus, under shear load boundary conditions the improvement in buckling performance is not entirely due to tow steering and this is mainly due to the effect of A_{16}, A_{26} distributions as a result of making the laminate unbalanced. The laminate can also be made unbalanced by choosing VAT layups instead of the 45° which can considerably improve the shear buckling performance compared with $[45_2, 45 \pm \langle T_0|T_1\rangle]_s$ laminates.

The shear buckling performance of rectangular composite layups $[60_2, 60 \pm \langle T_0|T_1\rangle]_s$ (aspect ratio = 3) are shown in Fig. 8. The layup $[60_2, 60 \pm \langle 90|10\rangle]_s$ under negative shear has higher buckling load compared to other composite layups. The buckling mode shape of the layup $[60_2, 60 \pm \langle 90|10\rangle]_s$ was evaluated using DQM and FE modelling and the results are shown in Fig. 9. Furthermore, the A_{16}, A_{26} stiffness coefficient distributions of the VAT plates play a critical part in the improvement of shear buckling performance. The computation of shear buckling load will be erroneous, if the effects of in-plane extension-shear coupling coefficients A_{16}, A_{26} are ignored and results in a lower buckling load. Thus, we conclude from this numerical study, the improvement in buckling performance under shear load can be achieved by tailoring the A_{16}, A_{26} distributions by designing symmetric unbalanced hybridised straight fibre-VAT laminates.

5.2. Buckling analysis under in-plane shear displacement

In this section, the buckling behaviour of VAT plates under shear displacement is investigated. The edges of the plate are kept straight during the application of shear displacement and the schematics of the VAT plate shown in Fig. 10 explains the applied displacement boundary conditions. The in-plane displacement boundary conditions are given by

$$\begin{aligned} x &= \pm\frac{a}{2}; \quad u = \mp\Delta_x, \quad v = \pm\Delta_y, \\ y &= \pm\frac{b}{2}; \quad u = -2\frac{\Delta_x}{a}x, \quad v = 2\frac{\Delta_y}{a}x, \end{aligned} \tag{25}$$

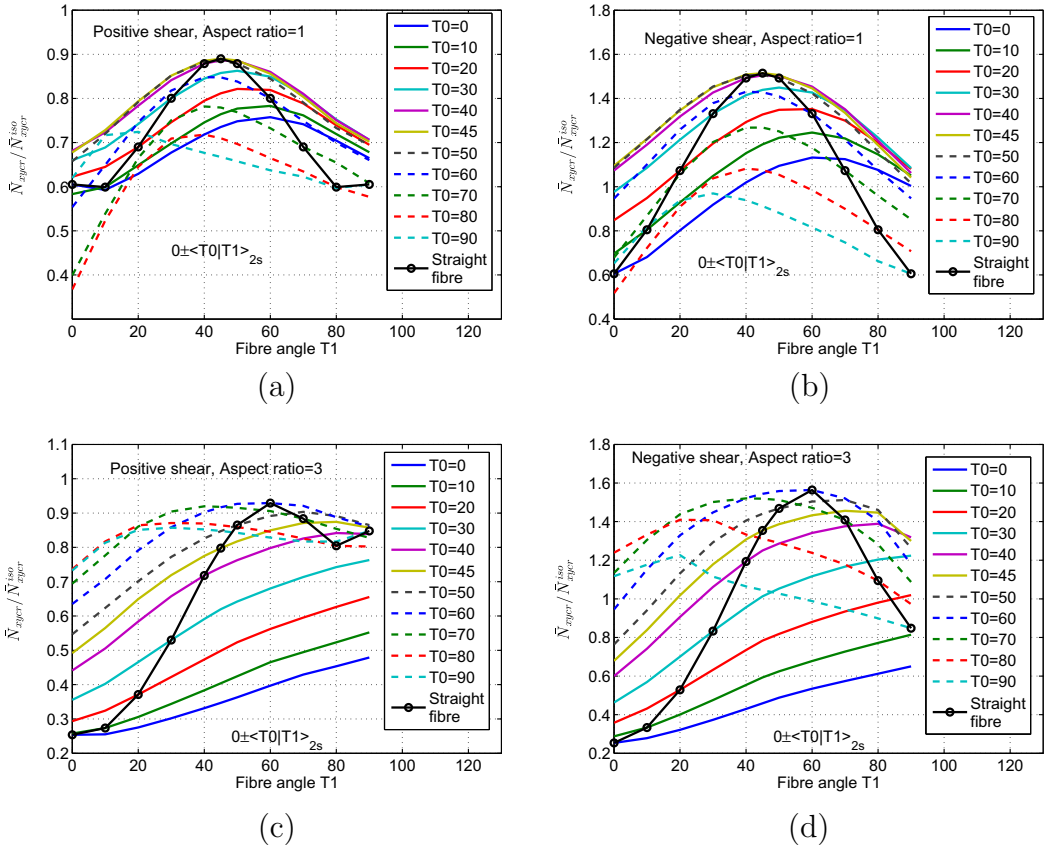

Fig. 4. Square VAT plate $0 \pm \langle T_0|T_1\rangle_{2s}$ subjected to in-plane shear load (a) positive shear, aspect ratio = 1 (b) negative shear, aspect ratio = 1 (c) positive shear, aspect ratio = 3 (d) negative shear, aspect ratio = 3.

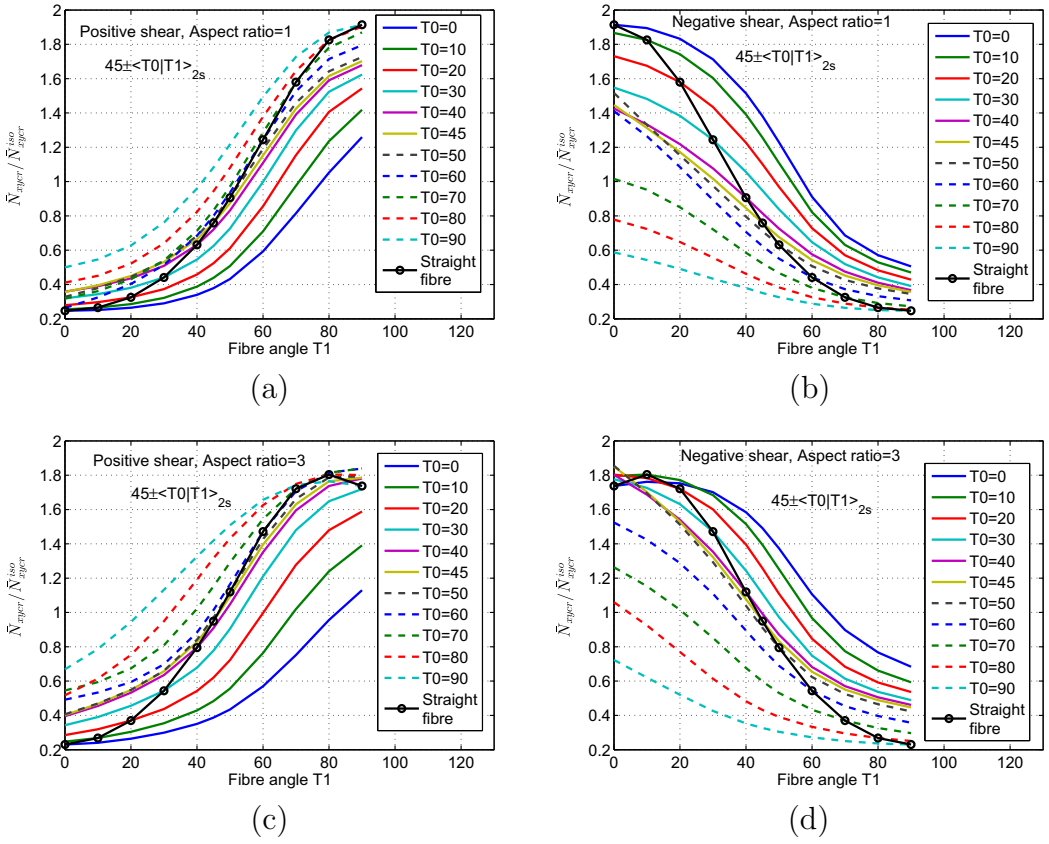

Fig. 5. Square VAT plate $45 \pm \langle T_0|T_1\rangle_{2s}$ subjected to in-plane shear load (a) positive shear, aspect ratio = 1 (b) negative shear, aspect ratio = 1 (c) positive shear, aspect ratio = 3 (d) negative shear, aspect ratio = 3.

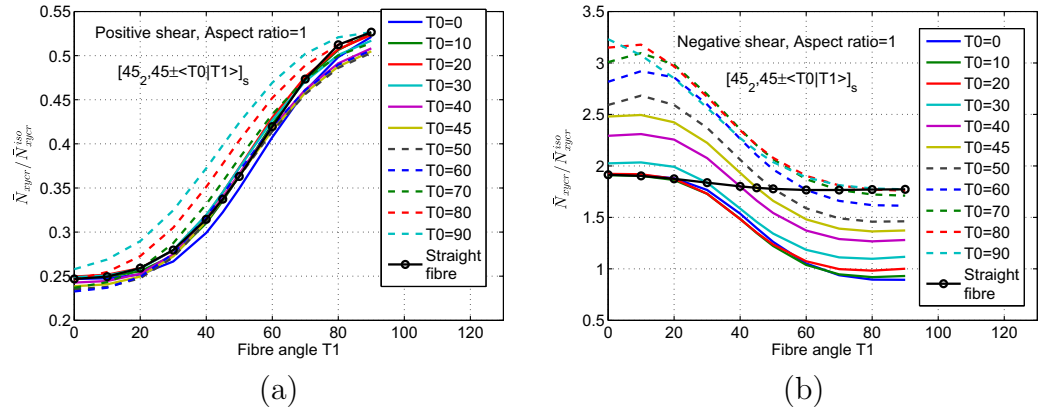

Fig. 6. Square VAT plate $[45_2, 45 \pm \langle T_0|T_1\rangle]_s$ subjected to in-plane shear load (a) positive shear, aspect ratio = 1 (b) negative shear, aspect ratio = 1.

where $\alpha = sin^{-1}\left(\frac{2\Delta_x}{a}\right)$, $\Delta_y = \frac{a}{2}(1 - cos\alpha)$ and Δ_x is the applied displacement magnitude. As the boundary conditions are specified solely in terms of displacements, DQM was applied to solve the in-plane coupled partial differential equations expressed in terms of displacements instead of the stress function based differential equation. Details of the GDEs expressed in terms of displacement u, v, w for solving the prebuckling, buckling and postbuckling problem of symmetric VAT plates are given in the Appendix. This approach was taken due to the difficulty in applying the displacement based conditions in terms of stress function, as they are expressed using integral expressions which are nonlocal boundary conditions and pose additional problems to satisfy them accurately at the boundary grid points. The DQM procedure discussed in the work of Groh and Weaver (2014) was used here to solve the prebuckling problem expressed in terms of in-plane displacements. The resulting DQM algebraic equations were solved for shear displacement boundary conditions and results in non-uniform stress resultant distributions for VAT plates. To determine the average shear buckling load applied to the VAT panel, it is essential to examine the contribution of each stress resultant in satisfying the specified displacement boundary conditions. For the edges to be straight, the stress resultants $\overline{N}_x$, $\overline{N}_y$ are nonzero along the edges and have

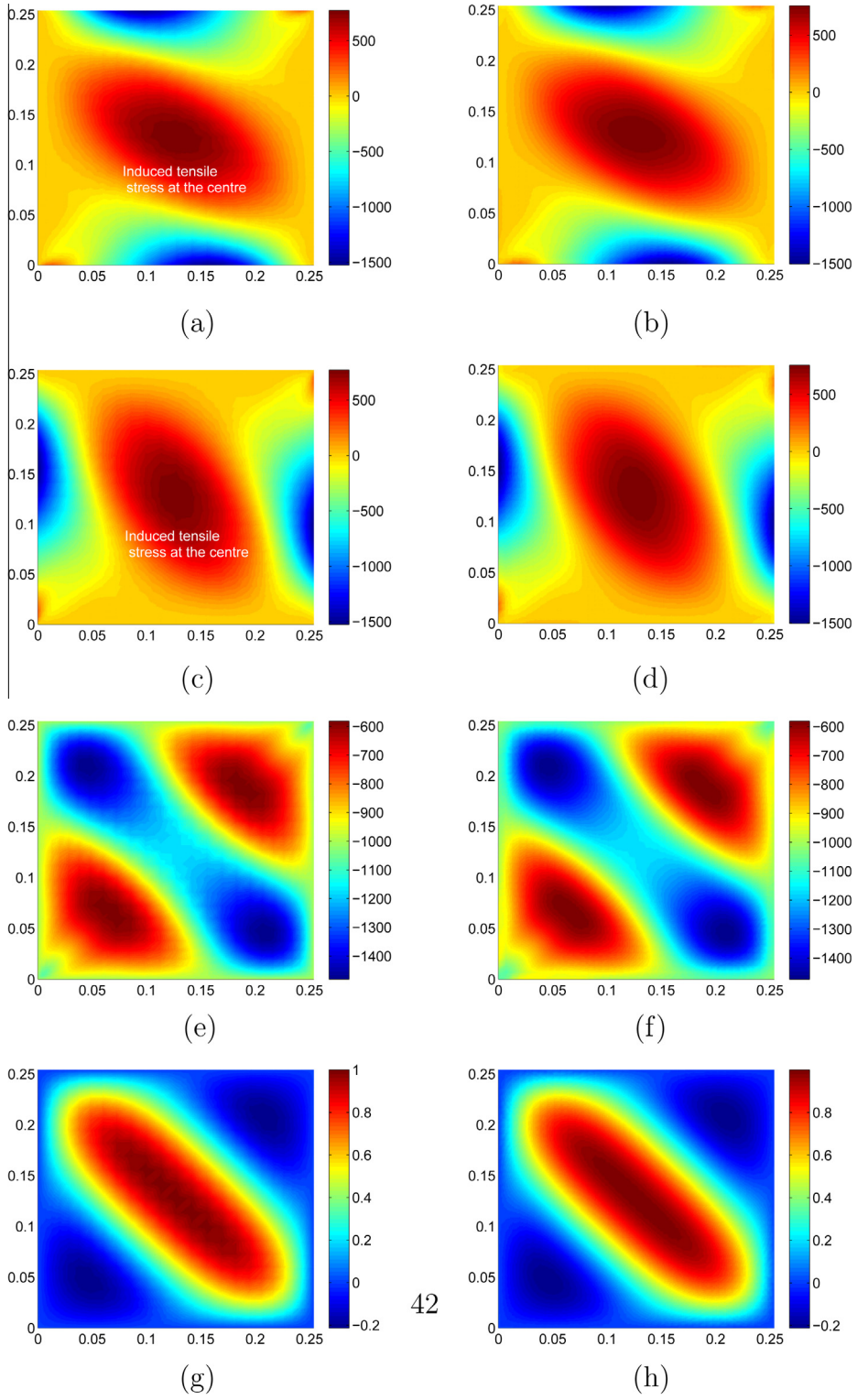

Fig. 7. Square VAT plate $[45_2, 45 \pm \langle 90|0 \rangle]_s$ subjected to in-plane negative shear load: stress resultant distribution $\overline{N}_x$ (a) DQM (b) FEM, stress resultant distribution $\overline{N}_y$ (c) DQM (d) FEM, stress resultant distribution $\overline{N}_{xy}$ (e) DQM (f) FEM, buckling mode shape (g) DQM (h) FEM.

considerable magnitude which cannot be ignored when compared to $\overline{N}_{xy}$ (Fig. 11). The non-zero stress resultants along the edges of the VAT plate result in moment distributions which have to be considered in evaluating the applied shear load. Detailed procedures for the computation of the moment due to stress resultants are explained in the work of Waldhart (1996). The moments due to $\overline{N}_x$, $\overline{N}_{xy}$ along edge $x = a/2$ and moments due to $\overline{N}_y$, $\overline{N}_{xy}$ along edge $y = b/2$ were used to compute the average applied shear resultant $\overline{N}_{xy}^{ave}$. The moments due to $\overline{N}_x$, $\overline{N}_y$, $\overline{N}_{xy}$ are defined as,

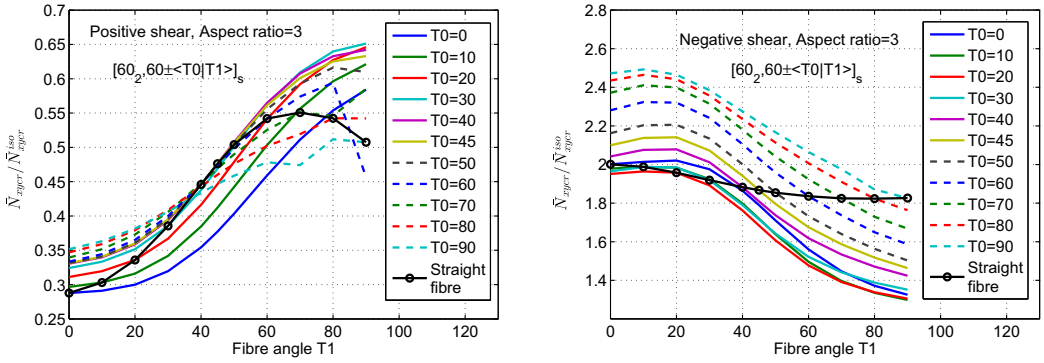

Fig. 8. Rectangular VAT plate $[60_2, 60 \pm \langle T_0|T_1\rangle]_s$ subjected to in-plane shear load (a) positive shear, aspect ratio = 1 (b) negative shear, aspect ratio = 3.

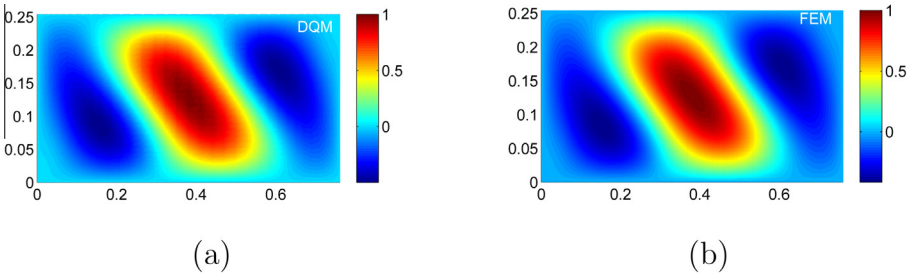

Fig. 9. Rectangular VAT plate $[60_2, 60 \pm \langle 90|10\rangle]_s$ subjected to in-plane negative shear load: Buckling mode shape (a) DQM (b) FEM.

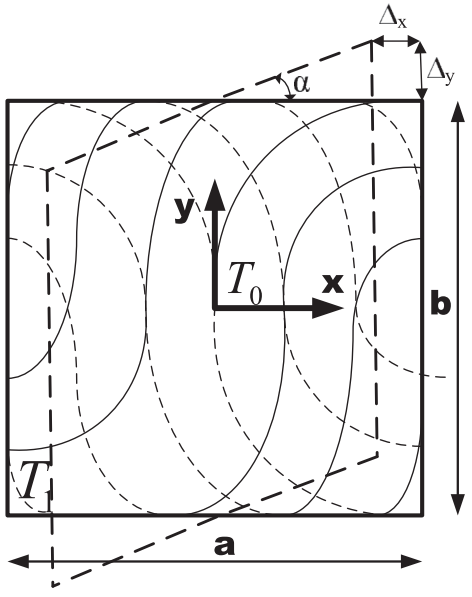

Fig. 10. Square VAT plate subjected to positive in-plane shear displacement.

$$
\begin{aligned}
M_z^i &= \int_{-b/2}^{b/2} y\overline{N}_x(a/2,y)dy,\\
M_z^{ii} &= -\int_{-a/2}^{a/2} x\overline{N}_y(x,b/2)dx,\\
M_z^{iii} &= -b/2\int_{-a/2}^{a/2} \overline{N}_{xy}(x,b/2)dx,\\
M_z^{iv} &= a/2\int_{-b/2}^{b/2} \overline{N}_{xy}(a/2,y)dy
\end{aligned}
\tag{26}
$$

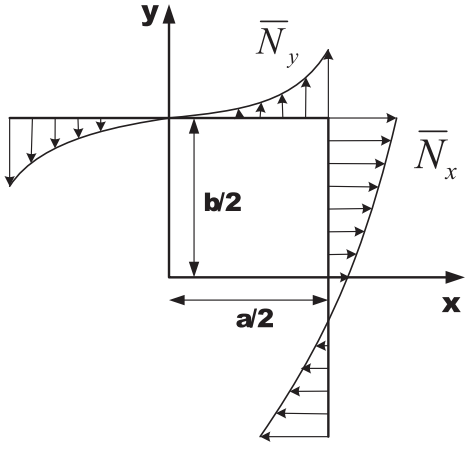

Fig. 11. VAT plate subjected to positive in-plane shear displacement: variation of $\overline{N}_x$ and $\overline{N}_y$ along the top and right edges of the plate.

where M_z^i is the moment about the z axis by the $\overline{N}_x$ acting along the edge $x = a/2$, M_z^{ii} is the moment about the z axis by the $\overline{N}_y$ acting along the edge $y = b/2$, and M_z^{iii}, M_z^{iv} are the moments about the z axis created by $\overline{N}_{xy}$ acting along the edges $x = a/2$, $y = b/2$, respectively. In this work, the moment in the anticlockwise direction is taken to be positive. Under positive shear deformation, M_z^{iii} is negative and M_z^{iv} is positive, but the sign of M_z^i, M_z^{ii} depends on the fibre path distribution and cannot be predetermined. Therefore, the positive and negative moments are given by,

$$
\begin{aligned}
M^+ &= M_z^{iv} + \begin{pmatrix} M_z^i, & M_z^i \geqslant 0 \\ 0, & M_z^i < 0 \end{pmatrix} + \begin{pmatrix} M_z^{ii}, & M_z^{ii} \geqslant 0 \\ 0, & M_z^{ii} < 0 \end{pmatrix},\\
M^- &= M_z^{iii} + \begin{pmatrix} 0, & M_z^i \geqslant 0 \\ M_z^i, & M_z^i < 0 \end{pmatrix} + \begin{pmatrix} 0, & M_z^{ii} \geqslant 0 \\ M_z^{ii}, & M_z^{ii} < 0 \end{pmatrix}.
\end{aligned}
\tag{27}
$$

The average of the moments M^+, M^- was used to compute the average shear load given by,

$$\overline{N}_{xy}^{ave} = \frac{1}{ab}\left(|M^+| + |M^-|\right). \tag{28}$$

The stress resultants obtained from the in-plane analysis of VAT plates were then used for computing the critical shear buckling load given by $\overline{N}_{xycr} = \lambda_{cr}\overline{N}_{xy}^{ave}$ where λ_{cr} is the minimum eigenvalue. The buckling performance of VAT plates under shear displacement was studied for different aspect ratios. The DQM grid size was chosen to be $N_x = N_y = 21$ for the square plate and $N_x = N_y = 25$ for plate with aspect ratio = 3 based on convergence studies. For VAT plates with $\phi = 0$ and various values of T_0, T_1, the normalised positive and negative shear buckling loads evaluated using DQM are shown in Fig. 12. For square VAT plates, the layup $0 \pm \langle 0|45\rangle_{2s}$ shows high positive and negative shear buckling load when compared to all other layups. For rectangular VAT plates, the layup $0 \pm \langle 90|45\rangle_{2s}$ shows better buckling performance than other layups. The VAT laminates considered until now are balanced and there is no effect of A_{16}, A_{26} stiffness coefficients on the shear buckling performance.

Next, we investigate the effects of A_{16}, A_{26} stiffness coefficients on the shear buckling performance of VAT laminates $\pm 45\langle T_0|T_1\rangle_{2s}$, $45 \pm \langle T_0|T_1\rangle_{2s}$ for different aspect ratios. Both the VAT layups $\pm 45\langle T_0|T_1\rangle_{2s}$, $45 \pm \langle T_0|T_1\rangle_{2s}$ have different fibre angle definitions based on the location of the ±sign with respect to the rotation angle ϕ (Waldhart, 1996). In the VAT layup $\pm 45\langle T_0|T_1\rangle_{2s}$, a ±sign in front of the ϕ means the reference fibre paths are rotated in equal and opposite amounts. For VAT layups $\pm 45\langle T_0|T_1\rangle_{2s}$, the fibre angle definition results in a balanced laminate in certain regions and unbalanced laminate elsewhere. This introduces finite A_{16}, A_{26} distributions in the VAT laminates. The normalised buckling load for VAT layups $\pm 45\langle T_0|T_1\rangle_{2s}$ was computed using DQM and is shown in Fig. 13 and the values are high compared to the straight fibre and VAT layups $0 \pm \langle T_0|T_1\rangle_{2s}$. This is primarily due to the redistribution of applied shear loads from the centre of the panel towards the edge and also the nonzero A_{16}, A_{26} stiffness distributions play a small role in improvement in buckling performance in either positive or negative shear direction.

For VAT layups $45 \pm \langle T_0|T_1\rangle_{2s}$, the fibre angle definition results in symmetric and unbalanced laminate configurations. These VAT laminates exhibit higher magnitude of A_{16}, A_{26} stiffness distributions because of their unbalanced layup sequence at each point. The shear buckling results of the VAT layups $45 \pm \langle T_0|T_1\rangle_{2s}$ are shown in Fig. 14 and exhibit some interesting behaviour. The term asymptotic buckling limit has been introduced to explain the buckling results shown in Fig. 14. An asymptotic buckling limit represents the VAT layup configuration $45 \pm \langle T_0|T_1\rangle_{2s}$ beyond which the VAT layups have effectively infinite shear buckling resistance (i.e. they do not buckle) in the negative or positive direction. In the case of VAT layup $45 \pm \langle 20|T_1\rangle_{2s}$, an asymptotic buckling load limit of 6.65 is attained at $T_1 = 60^\circ$ and exhibits effectively infinite shear buckling resistance for $T_0 = 20^\circ$ and $T_1 > 60^\circ$ in the positive shear direction. Similarly, VAT layup $45 \pm \langle 30|T_1\rangle_{2s}$ has an asymptotic buckling load limit of 16.15 at $T_1 = 80^\circ$ and infinite negative shear buckling resistance for $T_0 = 30^\circ$ and $T_1 > 80^\circ$. Another interesting observation is the large difference in the normalised buckling coefficient value, for example, between layups of similar configuration $45 \pm \langle 45|45\rangle_{2s}$ and $45 \pm \langle 40|45\rangle_{2s}$. This is due to the effect of A_{16}, A_{26} distributions in the VAT laminates. The $45 \pm \langle 45|45\rangle_{2s}$ layup is equivalent to a cross-ply layup with stiffness coefficients A_{16}, A_{26}. For VAT layup $45 \pm \langle 40|45\rangle_{2s}$, the

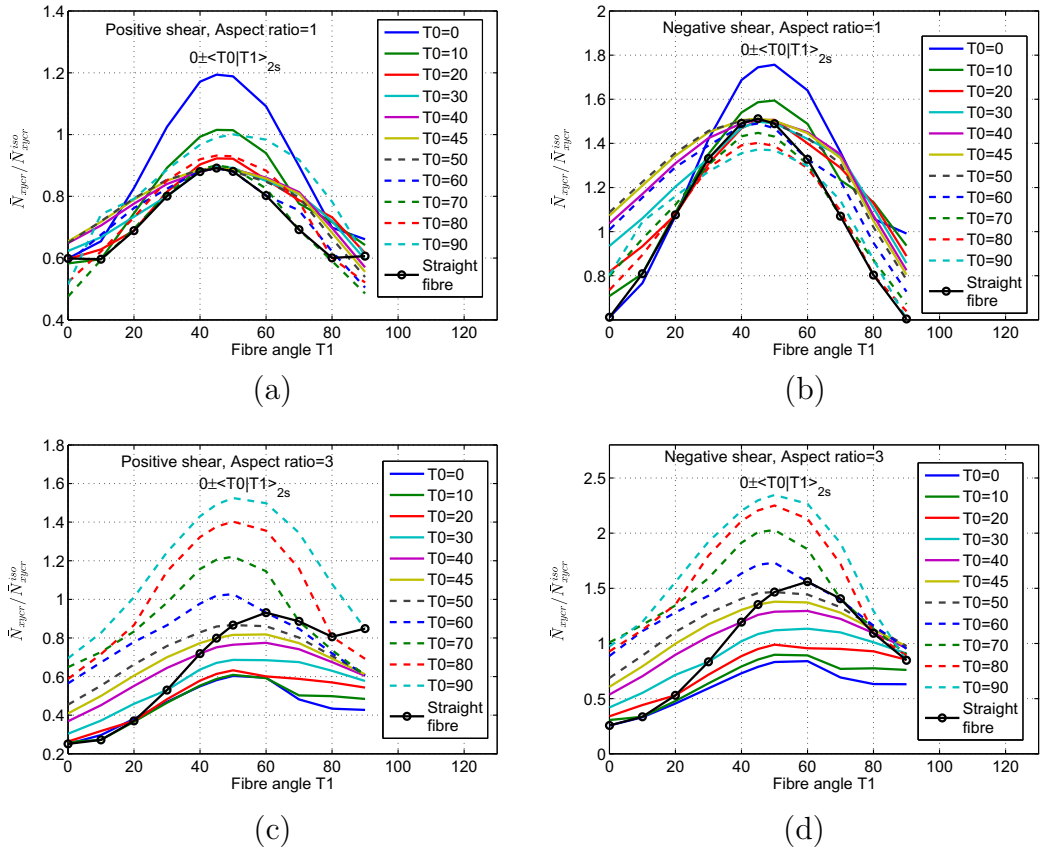

Fig. 12. Square VAT plate $0 \pm \langle T_0|T_1\rangle_{2s}$ subjected to in-plane shear displacement (a) positive shear, aspect ratio = 1 (b) negative shear, aspect ratio = 1 (c) positive shear, aspect ratio = 3 (d) negative shear, aspect ratio = 3.

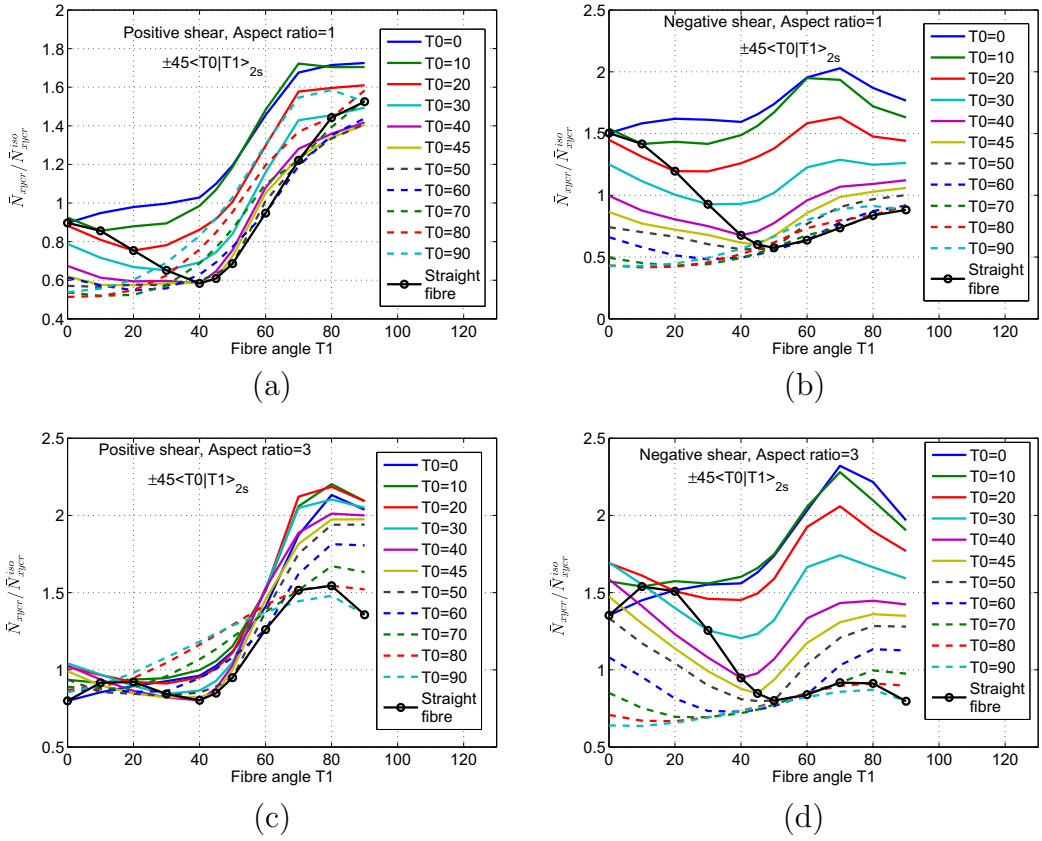

Fig. 13. Square VAT plate $\pm 45\langle T_0|T_1\rangle_{2s}$ subjected to in-plane shear displacement (a) positive shear, aspect ratio = 1 (b) negative shear, aspect ratio = 1 (c) positive shear, aspect ratio = 3 (d) negative shear, aspect ratio = 3.

laminates are unbalanced resulting in finite A_{16}, A_{26} distributions and they introduce $\overline{N}_x$, $\overline{N}_y$, $\overline{N}_{xy}$ distributions in the VAT laminate to keep the edges of the plate straight. These non-uniform pre-buckling stress resultants are responsible for the improvement in shear buckling load coefficient and for the difference in buckling results for similar VAT layup configurations.

The VAT layup $45 \pm \langle 30|80\rangle_{2s}$ has normalised buckling load coefficient of 16.15 under negative shear and the stress resultant distributions corresponding to this layup are shown in Fig. 15 such that the interior of the plate is effectively stress-free. The DQM results validate the FE modelling solutions and the stress resultant field shows the load redistribution towards the edges of the plate. The maximum and minimum principal stress resultants for the VAT layup $45 \pm \langle 30|80\rangle_{2s}$ are shown in Fig. 16 and show the compressive component of the applied shear being redistributed from the centre towards the plate edges. Under positive shear, the VAT layup $45 \pm \langle 20|60\rangle_{2s}$ has normalised buckling load coefficient of 6.65 and the stress resultant distribution corresponding to this layup is shown in Fig. 17 such that a stress-free state is observed at the centre of the plate. The stress resultant distributions shown in Figs. 15 and 17 indicate the load redistribution responsible for the improvement in shear buckling performance under negative and positive shear, respectively. For rectangular VAT plates, the layup $45 \pm \langle 30|90\rangle_{2s}$ has a high normalised buckling coefficient value of 5.56 and the corresponding mode shape computed using DQM is shown in Fig. 18. Furthermore, the A_{16}, A_{26} stiffness distributions have considerable effect on the pre-buckling stress redistribution of symmetric unbalanced VAT layups and are responsible for better buckling performance in either positive or negative shear direction. We conclude, from this study, that for shear buckling under displacement boundary conditions, the redistribution of applied load plays a primary role in improvement of shear buckling performance.

5.3. Postbuckling analysis under in-plane shear load

The DQM methodology was extended to perform postbuckling analysis of composite plates under uniform shear load. Initially, buckling analysis of VAT plates was performed to obtain the mode shape of the critical buckling load which is subsequently used as an imperfection function for the postbuckling analysis. For square VAT plates, the number of grid points for DQM modelling was chosen to be $N_x = N_y = 19$ based on a convergence study for accurate evaluation of the critical buckling load and mode shape (Raju et al., 2012). The imperfection function magnitude ($1E^{-5}$) for DQM was chosen to be the same as for FE modelling of the composite plate. For FE simulation, the mesh density of 40×40 was selected to analyse the above problem after a mesh convergence study. Subsequently, the postbuckling behaviour of different configurations of straight fibre and VAT laminates under uniform shear was studied. The normalised shear load versus normalised maximum transverse displacement for different composite plates is shown in Fig. 19 and the DQM results match FE solutions relatively well. The variation of maximum transverse deflection of the VAT plate with respect to the applied shear load shows the improved postbuckling performance under negative shear rather than positive shear load. The postbuckling performance of all VAT layups under positive shear were not as good as the QI layup. The VAT layups $45 \pm \langle 45|30\rangle_{2s}$, $45 \pm \langle 0|30\rangle_{2s}$ exhibit higher buckling load, but lower postbuckling performance than the QI layup under negative shear. The combined straight fibre and VAT layups $[45_2, 45 \pm \langle 90|0\rangle]_s$, $[45_2, 45 \pm \langle 45|0\rangle]_s$ show higher buckling load

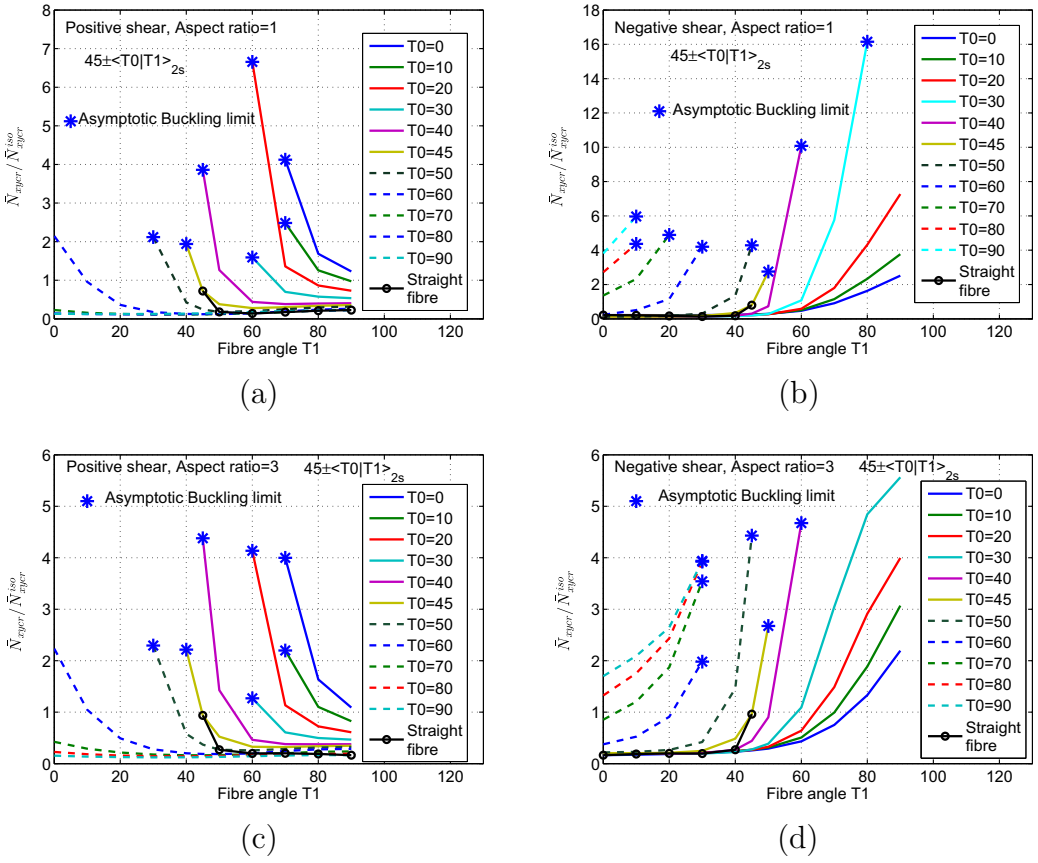

Fig. 14. Square VAT plate $45 \pm \langle T_0|T_1\rangle_{2s}$ subjected to in-plane shear displacement (a) positive shear, aspect ratio = 1 (b) negative shear, aspect ratio = 1 (c) positive shear, aspect ratio = 3 (d) negative shear, aspect ratio = 3.

and improved postbuckling performance under negative shear when compared to the QI layup.

DQM was then applied to study the postbuckling behaviour of rectangular plates (aspect ratio = 3) under negative shear. The number of grid points for DQM modelling was chosen to be $N_x = N_y = 25$ based on a convergence study. For FE modelling of rectangular VAT plates, a mesh density of 90×30 was selected. The DQM and FE results for different VAT plates are shown in Fig. 20. The straight fibre layup $[60]_8$ and VAT layup $45 \pm \langle 45|0\rangle_{2s}$ show better postbuckling performance compared to QI under negative shear. The postbuckling performance for combined straight fibre and VAT layups is investigated and the results are compared with VAT layups $\phi \pm \langle T_0|T_1\rangle_{2s}$ shown in Fig. 20. The layup $[60_2, 60 \pm \langle 90|10\rangle]_s$ exhibits better buckling and postbuckling performance and this improvement is significant as observed under axial compression for VAT laminates. Similar to the previously shown buckling behaviour, by tailoring the A_{16}, A_{26} distributions using symmetric unbalanced layups ($[45_2, 45 \pm \langle 90|0\rangle]_s$, $[45_2, 45 \pm \langle 45|0\rangle]_s$, $[60_2, 60 \pm \langle 90|10\rangle]_s$) has significant effect on their postbuckling performance.

5.4. Postbuckling analysis under in-plane shear displacement

In this section, the postbuckling behaviour of VAT plates subject to shear displacement boundary conditions is investigated. The GDEs for postbuckling analysis of VAT plates were expressed in terms of displacements u, v, w and the DQM procedure was applied to solve them. Similar to the DQM approach applied in solving Eqs. (7) and (9), the same numerical procedures were applied to convert the GDEs given in the Appendix into DQM form. The number of grid points for DQM modelling was chosen to be $N_x = N_y = 21$ for square plates based on a convergence study. The postbuckling results computed using DQM for both positive and negative shear displacement are shown in Fig. 21. The VAT layups exhibit better shear postbuckling performance compared to homogeneous QI and straight fibre layups. Under positive shear, the layup $45 \pm \langle 40|45\rangle_{2s}$ shows high postbuckling performance, but exhibits poor postbuckling performance under negative shear. Similarly, the layup $45 \pm \langle 30|70\rangle_{2s}$ shows good postbuckling performance in negative shear and poor performance in positive shear. The layup $\pm 45\langle 0|70\rangle_{2s}$ shows reasonably good postbuckling performance under positive and negative shear. Fig. 22 shows the results of VAT plates which have high buckling and postbuckling performance under positive or negative shear compared to all other layups. The DQM postbuckling results for rectangular VAT plates (aspect ratio = 3) under positive and negative shear displacement are shown in Fig. 23. The VAT layups $45 \pm \langle 40|45\rangle_{2s}$, $45 \pm \langle 30|90\rangle_{2s}$ show good buckling and postbuckling performance under positive and negative shear displacement respectively, but poor performance in the opposite loading direction. Many VAT layups exhibit good postbuckling performance under both positive and negative shear and the results of VAT plates $0 \pm \langle 90|45\rangle_{2s}$, $45 \pm \langle 45|90\rangle_{2s}$ show this behaviour. As observed under buckling, the tailoring of A_{16}, A_{26} distributions has a significant effect on the postbuckling performance under either positive or negative shear directions. The postbuckling results computed using DQM correlate well with FE results for square and rectangular VAT plates. The improved postbuckling results observed indicate that the benefits of tow steering is even more pronounced for shear displacement than shear load boundary conditions. The reason is attributed primarily to the phenomenon of load redistribution due to tow steering observed under

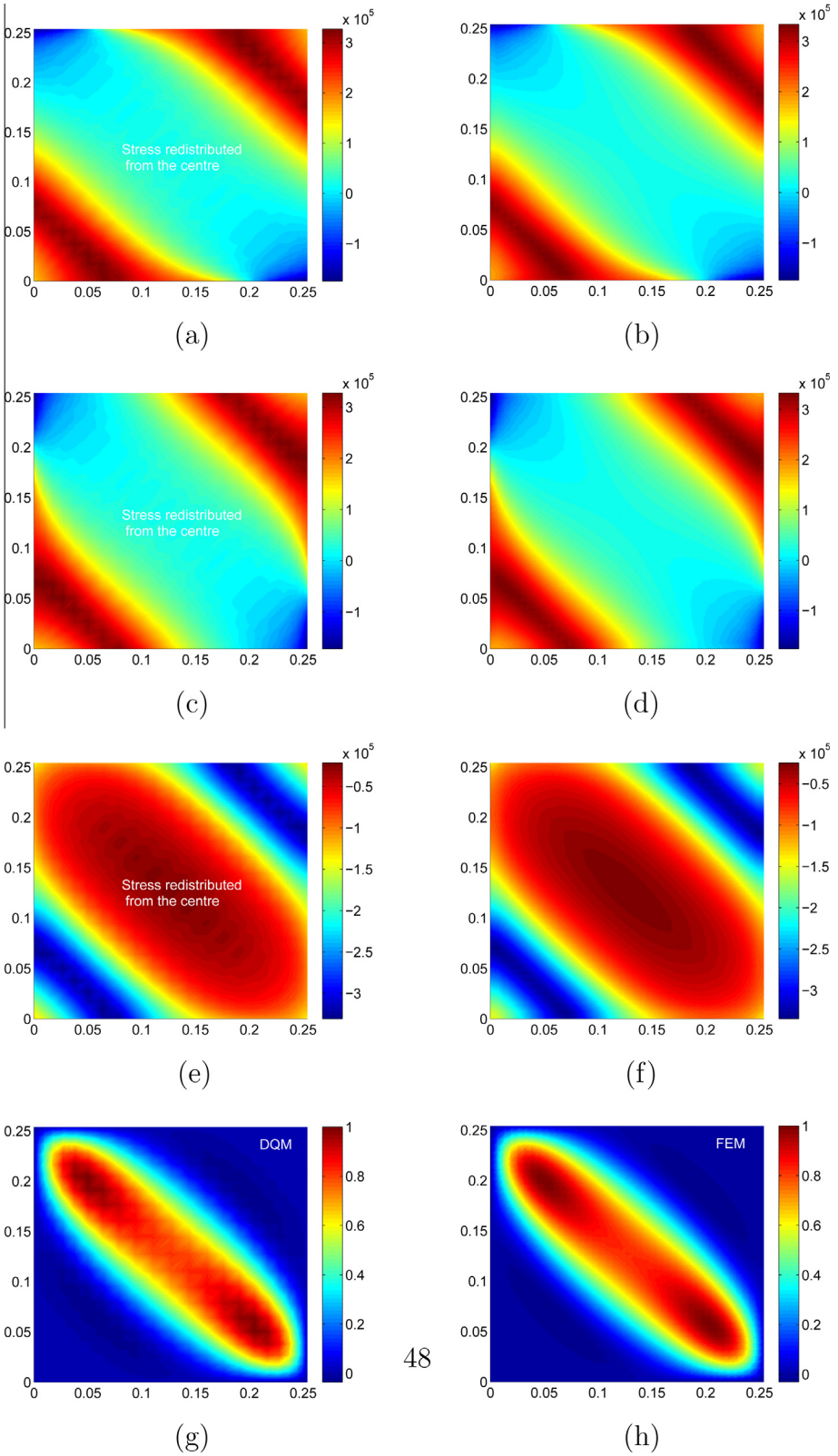

Fig. 15. Square VAT plate $[45 \pm \langle 30|80 \rangle]_{2s}$ subjected to in-plane negative shear displacement: stress resultant distribution $\overline{N}_x$ (a) DQM (b) FEM, stress resultant distribution $\overline{N}_y$ (c) DQM (d) FEM, stress resultant distribution $\overline{N}_{xy}$ (e) DQM (f) FEM, buckling mode shape (g) DQM (h) FEM.

prebuckling analysis. The prebuckling stress resultant distributions redistribute the local compressive stress from the centre towards the edge of the plate and during postbuckling analysis the stress distribution does not change much with the applied shear load.

5.5. Postbuckling analysis under combined axial compression and shear

The postbuckling behaviour of VAT plates under combined axial compression and shear was studied using DQM (Fig. 24). A square

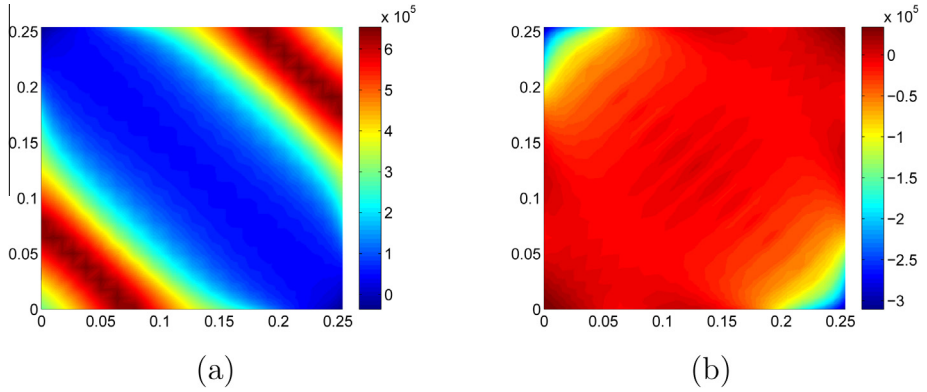

Fig. 16. Square VAT plate $[45 \pm \langle 30|80 \rangle]_{2s}$ subjected to in-plane negative shear displacement (a) maximum principal stress resultant (b) minimum principal stress resultant.

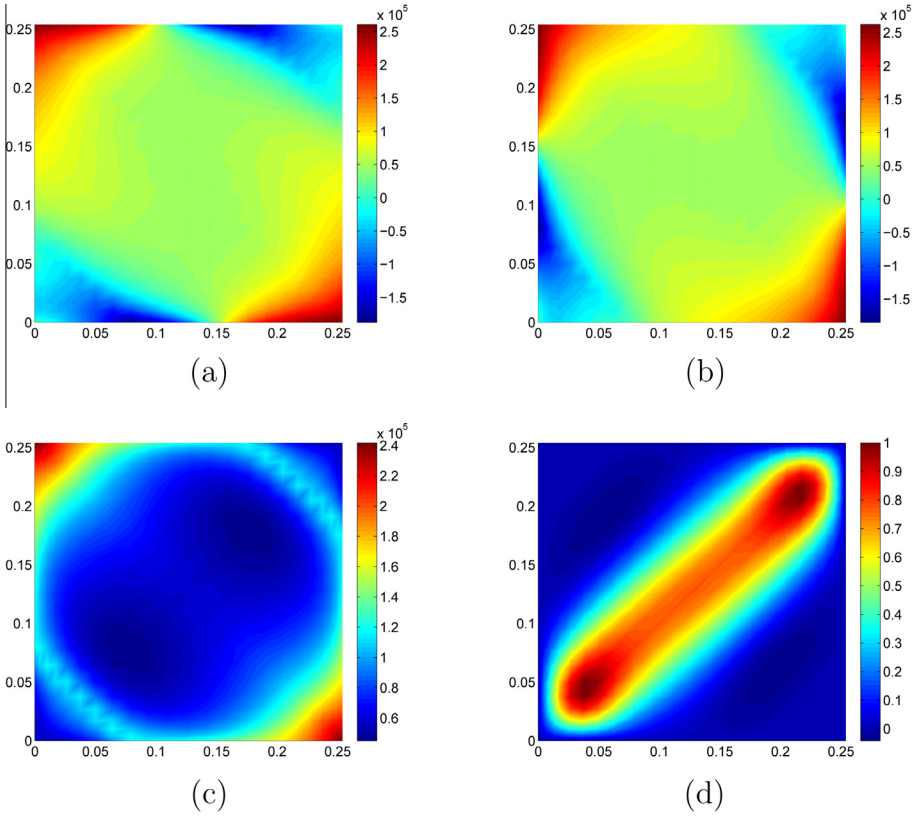

Fig. 17. Square VAT plate $[45 \pm \langle 20|60 \rangle]_{2s}$ subjected to in-plane positive shear displacement: (a) stress resultant distribution $\overline{N}_x$ (b) stress resultant distribution $\overline{N}_y$ (c) stress resultant distribution $\overline{N}_{xy}$ (d) buckling mode shape.

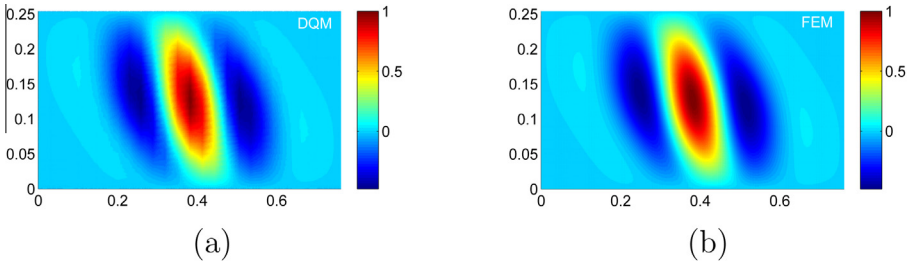

Fig. 18. Rectangular VAT plate $[45 \pm \langle 30|90 \rangle]_{2s}$ subjected to in-plane shear displacement: buckling mode shape (a) DQM (b) FEM.

VAT plate $(0 \pm \langle 45|30 \rangle_{2s})$ with a load ratio of $\overline{N}_{xy}/\overline{N}_x = 0.5$ was considered for the numerical study. The variation of maximum transverse centre deflection with increasing axial compression and shear is shown in Fig. 25. The direction of applied shear load has considerable influence on the postbuckling behaviour. The results show that negative shear improves slightly and positive shear

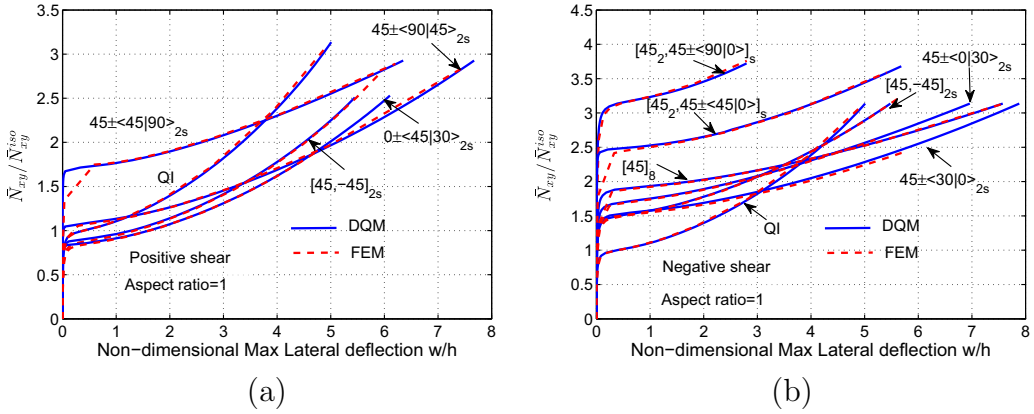

Fig. 19. Square VAT plate subjected to in-plane shear load: normalised applied shear load ($\overline{N}_{xy}/\overline{N}^{iso}_{xy}$) versus non-dimensional maximum lateral deflection w/h (a) positive shear (b) negative shear.

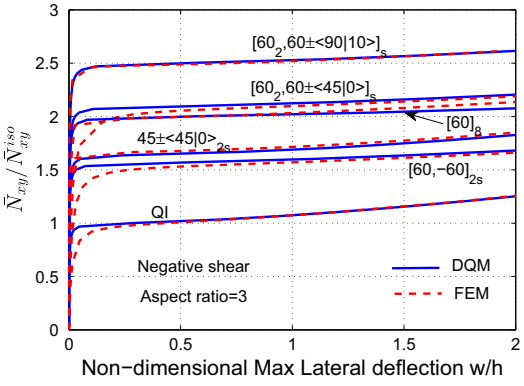

Fig. 20. Rectangular VAT plate (aspect ratio = 3) subjected to in-plane negative shear load: normalised applied shear load ($\overline{N}_{xy}/\overline{N}^{iso}_{xy}$) versus non-dimensional maximum lateral deflection w/h.

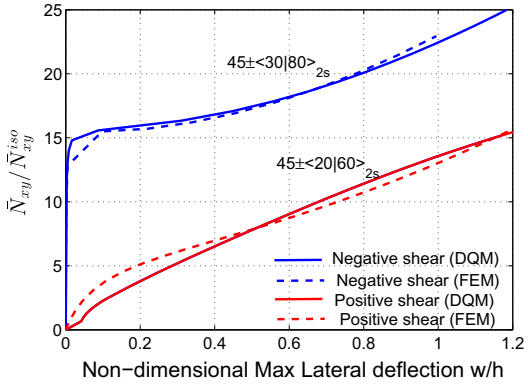

Fig. 22. Square VAT plate subjected to shear displacement: normalised applied shear load ($\overline{N}_{xy}/\overline{N}^{iso}_{xy}$) versus non-dimensional maximum lateral deflection w/h.

reduces the postbuckling performance of VAT plates. Next, a VAT plate ($90 \pm \langle 0|75 \rangle_{2s}$) which exhibits better buckling performance compared with straight fibre composites under axial compression was considered for the numerical study. The result shows that negative shear reduces the postbuckling performance and that positive shear has little effect (Fig. 26). This arises because the effect of shear loads is reversed for angle of rotation $\phi = 90^{\circ}$. Thus, the results show the influence of direction of shear load on the postbuckling performance under axial compression.

5.6. Discussion

In this work, the DQM approach was successfully applied to model the buckling and postbuckling behaviour of VAT plates under uniform in-plane shear load and displacement boundary conditions. For the linear shear buckling problem, DQM required few grid points and less computational effort to achieve converged results than the FE method. Similarly, for nonlinear postbuckling analysis, DQM modelling uses few grid points, but needs more iter-

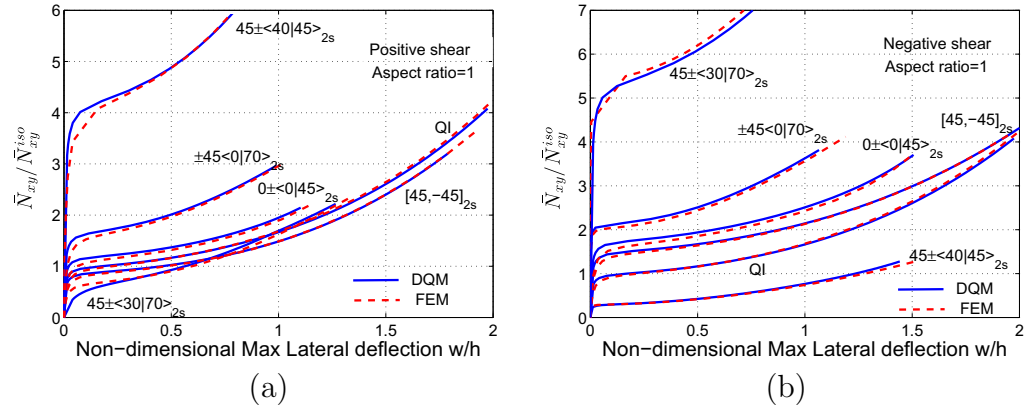

Fig. 21. Square VAT plate subjected to shear displacement: normalised applied shear load ($\overline{N}_{xy}/\overline{N}^{iso}_{xy}$) versus non-dimensional maximum lateral deflection w/h (a) positive shear (b) negative shear.

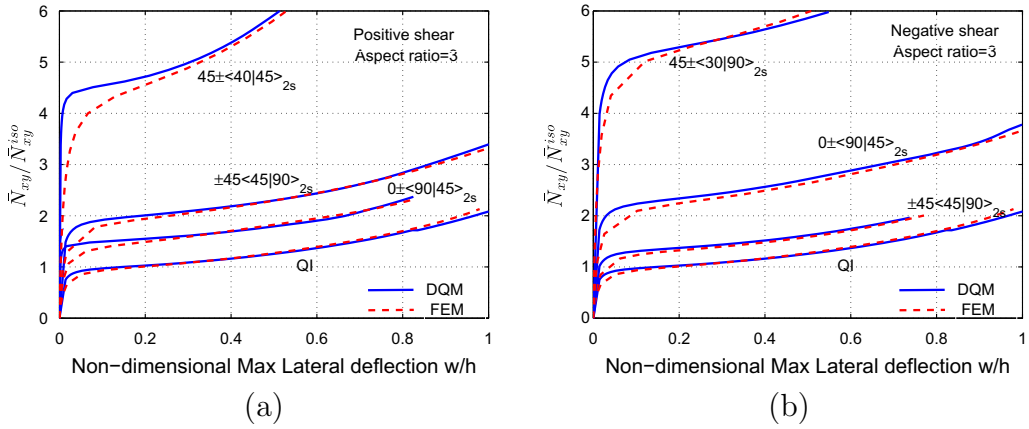

Fig. 23. Rectangular VAT plate (aspect ratio = 3) subjected to shear displacement: normalised applied shear load ($\overline{N}_{xy}/\overline{N}_{xy}^{iso}$) versus non-dimensional maximum lateral deflection w/h (a) positive shear (b) negative shear.

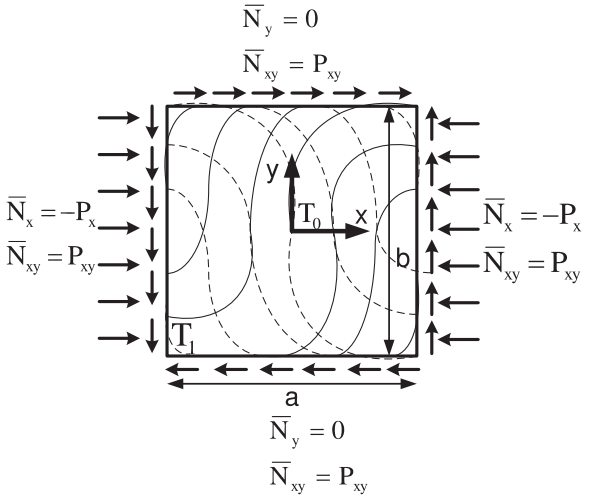

Fig. 24. Square VAT plate subjected to combined axial compressive and positive in-plane shear load.

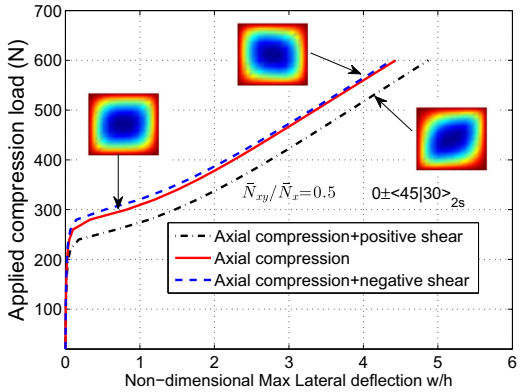

Fig. 25. Square VAT plate $0 \pm \langle 45|30\rangle_{2s}$ subjected to combined axial compression and shear load with load ratio $\overline{N}_{xy}/\overline{N}_x = 0.5$.

ations to converge in each load step when compared to FE modeling. This problem arises due to the nonsymmetric nature of the DQM stiffness matrix and also stronger reinforcement of all the boundary conditions at the boundary grid points. Although the DQM results were comparable to FE solutions, the method is not as general as FE modelling as it cannot be applied to structures with discontinuities/complicated geometry.

For shear load boundary conditions, the benefit for buckling and postbuckling response under negative shear is only observed when unbalanced VAT laminates are used such that a biaxial tensile stress (Fig. 7) is induced in the interior of the plate. Balanced VAT layups do not exhibit improved shear buckling and postbuckling behaviour in both directions as there is no load redistribution and secondary stress condition observed. Therefore, tailoring the finite A_{16}, A_{26} distributions of the hybridised unbalanced VAT laminates introduce favourable tensile stress states and improve the shear buckling and postbuckling performance in either positive or negative directions. In the case of shear displacement, balanced VAT layups exhibit improved buckling and postbuckling performance in positive and negative shear directions compared with straight fibre laminates. In addition for unbalanced VAT layups, the A_{16}, A_{26} stiffness distributions has considerable effect on the buckling and postbuckling performance in either the positive or negative shear direction. The phenomenon of redistribution of the applied shear load shown in Figs. 15 and 17 is mainly responsible for the improved shear buckling and postbuckling performance of VAT plates. Thus, the phenomena of induced secondary tensile stress state at the centre of the plate and achievement of stress-free state at the centre by redistribution of applied load towards the edges of the plate are responsible for the improvement of shear buckling and postbuckling performance under shear load-control and displacement-control boundary conditions, respectively. Furthermore, the buckling and postbuckling results of VAT laminates under shear displacement boundary conditions is more significant than observed under load-control.

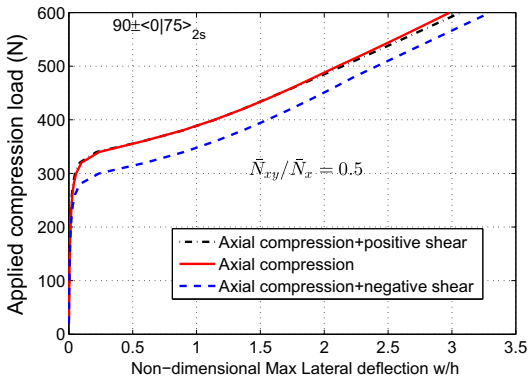

Fig. 26. Square VAT plate $90 \pm \langle 0|75\rangle_{2s}$ subjected to combined axial compression and shear load with load ratio $\overline{N}_{xy}/\overline{N}_x = 0.5$.

6. Conclusion

In this work, the buckling and postbuckling performance of symmetric VAT composite panels with linear fibre angle variation under in-plane shear is presented. The numerical results are computed using DQM for VAT plates with different aspect ratios and they correlate well with FE analysis. The numerical study show the effect of extension-shear coupling on the buckling and postbuckling performance of VAT composite plates under different in-plane boundary conditions. The physical understanding of the mechanics responsible for the improvement of buckling and postbuckling performance of VAT plates under shear load and displacement conditions is explained. Under constant shear load boundary condition, the linear fibre angle variation of VAT layups does not exhibit improved buckling and postbuckling behaviour. But, VAT layers combined with straight fibre layers result in improved buckling and postbuckling performance under negative shear, but poor performance under positive shear. The presence of induced tensile stresses in both x, y directions is responsible for the improved shear buckling and postbuckling performance under constant shear load. In the case of shear displacement, VAT layups exhibit improved buckling and postbuckling performance compared with straight fibre laminates. The redistribution of the applied shear load is responsible for the improved shear buckling and postbuckling performance of VAT plates. For shear displacement boundary conditions, the linear fibre angle variation allows simultaneous improvement of shear buckling and postbuckling performance under negative and positive shear. Furthermore, postbuckling behaviour of VAT plates under combined axial compression and in-plane shear was studied using DQM. The results shows the effect of the applied shear can be used to increase or decrease the postbuckling performance of VAT plates under combined loading conditions.

Acknowledgments

The authors would like to thank EPSRC, Airbus and GKN for supporting the work carried out under the ABBSTRACT2 project(EP/H026371/1).

Appendix A

The partial differential equations governing the postbuckling behaviour of symmetric VAT plates expressed in terms of displacements u, v, w are given by

$$\begin{aligned}
&A_{11}(x,y)u_{,xx} + 2A_{16}(x,y)u_{,xy} + A_{66}(x,y)u_{,yy} + (A_{11,x}(x,y)\\
&+ A_{16,y}(x,y))u_{,x} + (A_{16,x}(x,y) + A_{66,y}(x,y))u_{,y} + A_{16}(x,y)v_{,xx}\\
&+ (A_{12}(x,y) + A_{66}(x,y))v_{,xy} + A_{26}(x,y)v_{,yy} + (A_{16,x}(x,y)\\
&+ A_{66,y}(x,y))v_{,x} + (A_{12,x}(x,y) + A_{26,y}(x,y))v_{,y}(A_{11}(x,y)w_{0,x}\\
&+ A_{16}(x,y)w_{0,y})w_{,xx} + (A_{26}(x,y)w_{0,y} + A_{66}(x,y)w_{0,x})w_{,yy}\\
&+ ((A_{12}(x,y) + A_{66}(x,y))w_{0,y} + 2A_{16}(x,y)w_{0,x})w_{,xy} + \frac{1}{2}(A_{16,y}(x,y)\\
&+ A_{11,x}(x,y))w_{,x}^2 + \frac{1}{2}(A_{26,y}(x,y) + A_{12,x}(x,y))w_{,y}^2\\
&+ (A_{66}(x,y)w_{,yy} + 2A_{16}(x,y)w_{,xy} + (A_{11,x}(x,y) + A_{16,y}(x,y))w_{0,x}\\
&+ A_{11}(x,y)w_{,xx} + A_{66}(x,y)w_{0,yy} + (A_{66,y}(x,y) + A_{16,x}(x,y))w_{0,y}\\
&+ A_{11}(x,y)w_{0,xx} + 2A_{16}(x,y)w_{0,xy})w_{,x} + (A_{26}(x,y)w_{,yy}\\
&+ (A_{66,y}(x,y) + A_{16,x}(x,y))w_{,x} + (A_{12}(x,y) + A_{66}(x,y))w_{,xy}\\
&+ (A_{66,y}(x,y) + A_{16,x}(x,y))w_{0,x} + A_{26}(x,y)w_{0,yy} + A_{16}(x,y)w_{,xx}\\
&+ (A_{12,x}(x,y) + A_{26,y}(x,y))w_{0,y} + A_{16}(x,y)w_{0,xx} + (A_{12}(x,y)\\
&+ A_{66}(x,y))w_{0,xy})w_{,y} = 0, \qquad (29)
\end{aligned}$$

$$\begin{aligned}
&A_{16}(x,y)u_{,xx} + (A_{12}(x,y) + A_{66}(x,y))u_{,xy} + A_{26}(x,y)u_{,yy}\\
&+ (A_{16,x}(x,y) + A_{12,y}(x,y))u_{,x} + (A_{66,x}(x,y) + A_{26,y}(x,y))u_{,y}\\
&+ A_{66}(x,y)v_{,xx} + 2A_{26}(x,y)v_{,xy} + A_{22}(x,y)v_{,yy} + (A_{66,x}(x,y)\\
&+ A_{26,y}(x,y))v_{,x} + (A_{26,x}(x,y) + A_{22,y}(x,y))v_{,y} + (A_{16}(x,y)w_{0,x}\\
&+ A_{66}(x,y)w_{0,y})w_{,xx} + (A_{26}(x,y)w_{0,x} + A_{22}(x,y)w_{0,y})w_{,yy}\\
&+ ((A_{12}(x,y) + A_{66}(x,y))w_{0,x} + 2A_{26}(x,y)w_{0,y})w_{,xy}\\
&+ \frac{1}{2}(A_{12,y}(x,y) + A_{16,x}(x,y))w_{,x}^2 + \frac{1}{2}(A_{22,y}(x,y) + A_{26,x}(x,y))w_{,y}^2\\
&+ (A_{26}(x,y)w_{0,yy} + (A_{12}(x,y) + A_{66}(x,y))w_{,xy} + (A_{16,x}(x,y)\\
&+ A_{12,y}(x,y))w_{0,x} + A_{26}(x,y)w_{,yy} + (A_{12}(x,y) + A_{66}(x,y))w_{0,xy}\\
&+ A_{16}(x,y)w_{,xx} + (A_{66,x}(x,y) + A_{26,y}(x,y))w_{0,y} + A_{16}(x,y)w_{0,xx})w_{,x}\\
&+ (A_{22}(x,y)w_{,yy} + (A_{66,x}(x,y) + A_{26,y}(x,y))w_{,x} + 2A_{26}(x,y)w_{,xy}\\
&+ A_{22}(x,y)w_{0,yy} + (A_{66,x}(x,y) + A_{26,y}(x,y))w_{0,x} + A_{66}(x,y)w_{,xx}\\
&+ 2A_{26}(x,y)w_{0,xy} + (A_{22,y}(x,y) + A_{26,x}(x,y))w_{0,y}\\
&+ A_{66}(x,y)w_{0,xx})w_{,y} = 0, \qquad (30)
\end{aligned}$$

$$\begin{aligned}
&D_{11}(x,y)w_{,xxxx} + 4D_{16}(x,y)w_{,xxxy} + 2(D_{12}(x,y) + 2D_{66}(x,y))w_{,xxyy}\\
&+ 4D_{26}(x,y)w_{,yyyx} + D_{22}(x,y)w_{,yyyy} + 2(D_{11,x}(x,y)\\
&+ D_{16,y}(x,y))w_{,xxx} + (6D_{16,x}(x,y) + 2D_{12,y}(x,y) + 4D_{66,y}(x,y))w_{,xxy}\\
&+ (2D_{12,x}(x,y) + 4D_{66,x}(x,y) + 6D_{26,y}(x,y))w_{,xyy} + 2(D_{26,x}(x,y)\\
&+ D_{22,y}(x,y))w_{,yyy} + (D_{11,xx}(x,y) + 2D_{16,xy}(x,y) + D_{12,yy}(x,y))w_{,xx}\\
&+ (2D_{16,xx}(x,y) + 4D_{66,xy}(x,y) + 2D_{26,yy}(x,y))w_{,xy} + (D_{12,xx}(x,y)\\
&+ 2D_{26,xy}(x,y) + D_{22,yy}(x,y))w_{,yy} - \bar{N}_x(w_{,xx} + w_{0,xx})\\
&- 2\bar{N}_{xy}(w_{,xy} + w_{0,xy}) - \bar{N}_y(w_{,yy} + w_{0,yy}) + q = 0. \qquad (31)
\end{aligned}$$

References

Bellman, R.E., Casti, J., 1971. Differential quadrature and long-term integration. J. Math. Anal. Appl. 34, 235–238.
Biggers, S.B., Fageau, S.S., 1994. Shear buckling response of tailored rectangular composite plates. AIAA J. 32 (5), 1100–1103.
Chen, W., Shu, C., He, W., Zhong, T., 2000. The application of special matrix product to differential quadrature solution of geometrically nonlinear bending of orthotropic rectangular plates. Compos. Struct. 74, 65–76.
Chu, K.T., 2009. A direct matrix method for computing analytical jacobian of discretized nonlinear intergro-differential equations. J. Comput. Phys. 228, 5526–5538.
Diaconu, C.G., Weaver, P.M., 2006. Postbuckling of long unsymmetrically laminated composite plates under axial compression. Int. J. Solids Struct. 43 (22–23), 6978–6997.
Gomes, V.S., Lopes, C.S., Pires, F.F.A., Grdal, Z., Camanho, P.P., 2013. Fibre steering for shear-loaded composite panels with cutouts. J. Compos. Mater., 0021998313492356
Groh, R.M.J., Weaver, P.M., 2014. Buckling analysis of variable angle tow, variable thickness panels with transverse shear effects. Compos. Struct. 107, 482–493.
Gurdal, Z., Olmedo, R., 1993. In-plane response of laminates with spatially varying fiber orientations: variable stiffness concept. AIAA J. 31 (4), 751–758.
Gurdal, Z., Tatting, B.F., Wu, C.K., 2008. Variable stiffness composite panels: effects of stiffness variation on the in-plane and buckling response. Compos.: Part A 39, 911–922.
Hyer, M.W., Lee, H.H., 1991. The use of curvilinear fiber format to improve buckling resistance of composite plates with central circular holes. Compos. Struct. 18, 239–261.
Jones, R.M., 1998. Mechanics of Composite Materials, second ed. CRC Press.
Lopes, C.S., Gurdal, Z., Camanho, P.P., 2010. Tailoring for strength of composite steered-fibre panels with cutouts. Compos.: Part A 41, 1760–1767.
Nemeth, M., 1997. Buckling behaviour of long symmetrically laminated plates subjected to shear and linearly varying axial edge loads. NASA technical paper, 3659.
Pandey, M.D., Sherbourne, A.N., 1993. Postbuckling behaviour of optimised rectangular composite laminates. Compos. Struct. 23, 27–38.
Rahman, T., IJsselmuiden, S.T., Abdalla, M.M., 2011. Postbuckling analysis of variable stiffness composite plates using a finite-element based perturbation method. Int. J. Struct. Stab. Dyn. 11 (4), 735–753.
Raju, G., Wu, Z., Weaver, P.M., 2012. Prebuckling and buckling analysis of variable angle tow plates with general boundary conditions. Compos. Struct. 94 (9), 2961–2970.
Raju, G., Wu, Z., Weaver, P.M., 2013. Postbuckling analysis of variable angle tow plates using differential quadrature method. Compos. Struct. 106, 74–80.

Shu, C., 2000. Differential Quadrature and Its Application in Engineering. Springer-Verlag, London.
Shu, C., Chen, W., 1999. On optimal selection of interior points for applying discretized boundary conditions in DQ vibration analysis of beams and plates. J. Sound Vib. 222 (2), 239–257.
Shu, C., Du, H., 1997. Implementation of clamped and simply supported boundary conditions in the GDQ free vibration analysis of beams and plates. Int. J. Solids Struct. 34, 819–835.
Taheri, F., Moradi, S., 2000. A robust methodology for the simulation of postbuckling response of composite plates. Comput. Mech. 26, 295–301.
Waldhart, C., 1996. Analysis of Tow-placed Variable Stiffness Laminates (MSc thesis). Virginia Tech.
Weaver, P.M., 2004. On optimisation of long anisotropic flat plates subject to shear buckling loads. In: 45th AIAA/ASME/ASCE/AHS/ASC Structures, Structural Dynamics, and Materials Conference.
Weaver, P.M., Nemeth, M.P., 2007. Bounds on flexural properties and buckling response for symmetrically laminated composite plates. J. Eng. Mech. 113 (11), 1178–1191.
Whitney, J.M., 1987. Structural Analysis of Laminated Anisotropic Plates. Technomic Publishing, PA, USA.
Wu, Z., Raju, G., Weaver P.M., 2012. Buckling of VAT plates using energy methods. In: 53rd AIAA/ASME/ASCE/AHS/ASC Structures, Structural Dynamics, and Materials Conference.
Wu, Z., Raju, G., Weaver, P.M., 2013. Postbuckling analysis of variable angle tow plates. Int. J. Solids Struct. 50 (10), 1770–1780.